CENTRO POLITÉCNICO SUPERIOR

UNIVERSIDAD DE ZARAGOZA

TRABAJO FIN DE MASTER

MECÁNICA APLICADA

POSTGRADO DE INGENIERÍAS MECÁNICA Y DE MATERIALES

CARACTERIZACIÓN MECÁNICA Y MODELADO NUMÉRICO DE LA PARED ABDOMINAL. DESARROLLO DE UNA METODOLOGÍA DE AYUDA AL DISEÑO DE MALLAS SINTÉTICAS PARA LA REPARACIÓN HERNIARIA.

AUTOR:

Belén Hernández Gascón

DIRECTOR:

Begoña Calvo Calzada

Departamento de Ingeniería Mecánica

Curso 2009/2010 - Septiembre 2010

Caracterización mecánica y modelado numérico de la pared abdominal. Desarrollo de una metodología de ayuda al diseño de mallas sintéticas para la reparación herniaria.

RESUMEN

La cirugía abdominal mediante la implantación de mallas sintéticas es la más utilizada para la reparación de hernias, pero estas mallas pueden causar varios problemas a los pacientes. Hoy en día, existe una gran variedad de mallas y no está científicamente demostrado cuál es la prótesis ideal ni cuáles son las pautas de orientación de las mismas en el cuerpo humano cuando se trata de mallas anisótropas. Las prótesis actuales han sufrido modificaciones en su estructura y su porosidad en los últimos tiempos con el objetivo de mejorar su adaptación al tejido. A pesar de estas mejoras, la "prótesis ideal" no ha sido obtenida, siendo común la reaparición de las hernias. Para entender el fenómeno es esencial que se caracterize mecánicamente la pared abdominal.

Para entender dicho comportamiento es necesario distinguir entre las fibras de colágeno y las musculares, porque en el tejido del músculo, las fibras de colágeno son las responsables de la resistencia mecánica y rigidez y las fibras musculares de la contracción. La dirección de las fibras de colágeno determinan la dirección de anisotropía del material, propiedad a tener en cuenta posteriormente en la formulación del modelo constitutivo. Debido a la distinta orientación de las fibras en cada capa (fibras musculares y de colágeno), en este estudio se analiza la influencia del estudio de las capas separadas en comparación con el músculo en conjunto considerándolo como un material compuesto.

Una vez que se ha entendido el comportamiento mecánico del músculo, se caracterizan tres mallas quirúrgicas utilizadas en la reparación herniaria. A su vez, se compara su comportamiento con el de la pared abdominal para estudiar qué malla es la que mejor reproduce el comportamiento de la pared abdominal.

En el contexto del modelado matemático, se ha definido un modelo constitutivo 3D hiperelástico anisótropo cuasi-incompresible para el músculo abdominal y otro 2D para las mallas. Utilizando los datos experimentales y realizando un ajuste numérico se han obtenido un conjunto de parámetros, para la función densidad de energía planteada en cada caso, que son capaces de reproducir el comportamiento real del músculo abdominal y de cada una de las mallas mediante un modelo de elementos finitos (FE).

En último lugar, con el objetivo de reproducir el comportamiento del abdomen sin dañar y el abdomen que ha sufrido una cirugía abdominal, se plantea un modelo simplificado de elementos finitos que simula el abdomen del animal de experimentación utilizado sometido a una presión abdominal interna. Con este modelo se trata de ver cómo se comporta el conjunto del abdomen bajo la presencia de las diferentes mallas estudiadas.

Caracterización mecánica y modelado numérico de la pared abdominal. Desarrollo de una metodología de ayuda al diseño de mallas sintéticas para la reparación herniaria.

RESUMEN DEL TFM

La cirugía abdominal por medio de la implantación de mallas sintéticas es la más frecuentemente utilizada para la reparación de hernias, entendidas como una protusión de una víscera a través de una abertura en la pared abdominal que la contiene, Figura 1. Estas mallas pueden causar varios problemas: molestias en pacientes porque la rigidez de la malla no es como la del músculo abdominal, reacción inflamatoria o creación de adhesiones entre el material implantado y los órganos. Hoy en día, hay una gran variedad de mallas ofrecidas en el mercado y no está científicamente demostrado cuál es la prótesis ideal para la reparación de hernias ni cuáles son las pautas de orientación de las mismas en el cuerpo humano cuando se trata de mallas anisótropas.

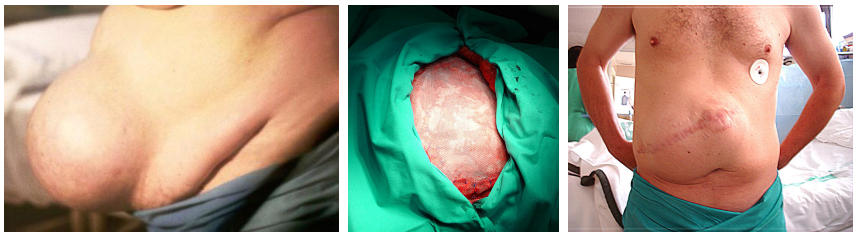

(a) (b) (c)

Figure 1: (a) Ejemplo de hernia abdominal. (b) Cirugía abdominal para la reparación herniaria por medio de la implantación de malla sintética. (c) Hernia en (a) curada .

Para la reparación de los tejidos el polipropileno es todavía el material preferido. Sin embargo, a lo largo de los años este material ha sufrido modificaciones en su estructura y su porosidad con el objetivo de mejorar su adaptación al tejido. Estos cambios han intentado reducir la creacción de cuerpos extraños y la fibrosis provocada en el lugar del implante. A pesar de estas mejoras, la “prótesis ideal” en términos de tamaño de poro y

estructura espacial que se adapte bien a las condiciones mecánicas del tejido no ha sido obtenida, siendo común la reaparición de las hernias. Para entender el fenómeno es esencial que se analice el lugar del implante, en el caso de estudio, la pared abdominal, realizando la caracterización mecánica de la misma. Por tanto, utilizando conejos como modelo de experimentación, se ha caracterizado mecánicamente la pared lateral del abdomen (Figura 2), mediante ensayos uniaxiales, como un estudio preliminar anterior al implante.

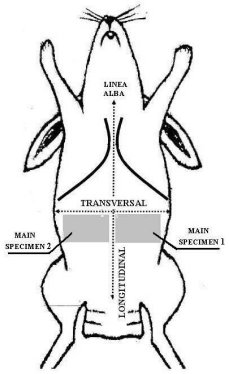

Figure 2: Modelo de experimentación animal para la caracterización de la pared abdominal. Definición de las direcciones longitudinal y transversal.

La pared abdominal contiene cuatro músculos expiratorios: el recto mayor, el oblicuo externo (EO), el oblicuo interno (IO) y el transverso (TA). Anatómicamente, el IO queda dispuesto internamente al EO en la pared abdominal lateral, mientras que el TA es el músculo abdominal más interno. Debido a la orientación de las fibras del músculo, el comportamiento es diferente en ambas direcciones, longitudinal (dirección craneo-caudal del conejo) y transversal (perpendicular a la longitudinal).

Relacionado con el comportamiento del modelo, el tejido del músculo es considerado como una red de fibras musculares, colágeno y elastina embebidas en una matriz mas o menos isótropa. Es necesario distinguir entre las fibras de colágeno y las musculares, porque en el tejido del músculo, las fibras de colágeno son las responsables de la resistencia mecánica y rigidez y las fibras musculares de la contracción. Para el tejido abdominal, el ángulo entre las fibras musculares y las de colágeno es distinto de cero. La dirección de las fibras de colágeno determinan la dirección de anisotropía del material para desarrollar posteriormente la formulación del modelo constitutivo. El estudio de la dirección de las fibras de colágeno y musculares se refuerza mediante un estudio histológico de la zona de estudio en la pared abdominal. Este estudio ha sido realizado y cedido por la Universidad de Medicina de Alcalá.

Debido a la distinta orientación de las fibras en cada capa (fibras musculares y de colágeno), en este estudio se analiza la influencia del estudio de las capas separadas en

comparación con el músculo en conjunto considerándolo como un material compuesto. Al mismo tiempo, es necesario conocer el comportamiento de la capas de músculo EO debido a que en la reparación de hernias parciales sólo se reemplaza dicha capa muscular. Los resultados de los ensayos uniaxiales se presentan graficando la tensión de Cauchy frente al alargamiento (λ), Figura 3.

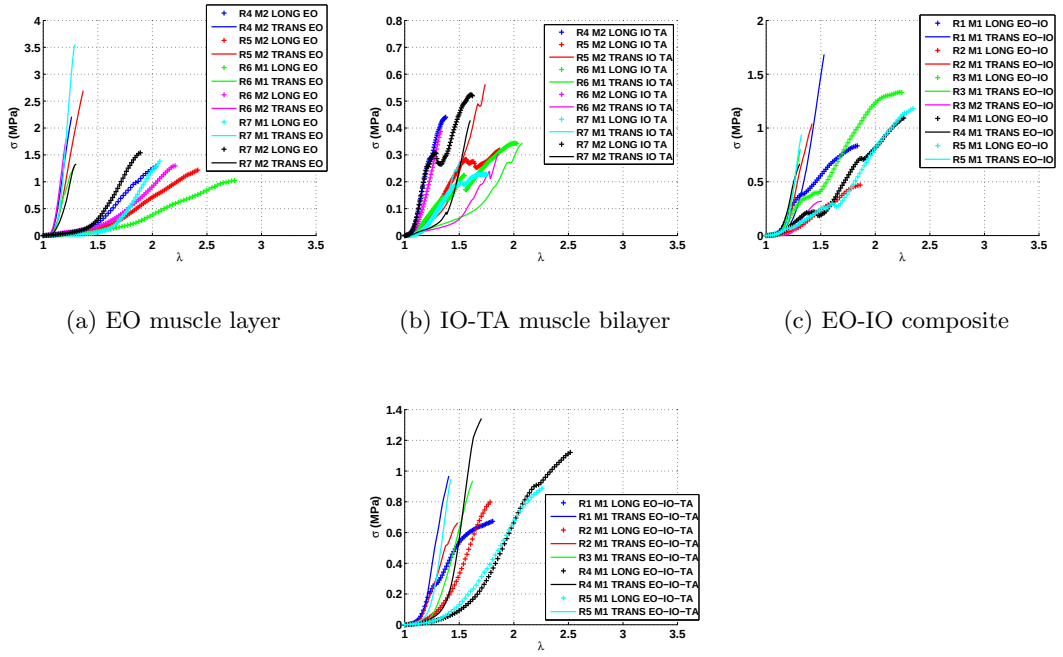

(a) EO muscle layer

(b) IO-TA muscle bilayer

(c) EO-IO composite

(d) EO-IO-TA composite

Figure 3: Datos experimentales para las distintas probetas estudiadas mediante ensayos uniaxiales. Todas las curvas se cortan en el punto de la tensión de rotura.

Respecto al comportamiento mecánico del músculo, se obtiene que las capas por separado presentan una alta anisotropía mientras que el músculo estudiado como un compuesto tiene un comportamiento intermedio, pero mostrándose la dirección transversal más rígida que la longitudinal. Esto se justifica debido a la existencia de una fuerza de transmisión miofascial entre capas que permite la transmisión de esfuerzos.

En el contexto del modelado matemático, se ha definido un modelo constitutivo 3D hiperelástico anisótropo cuasi-incompresible para el músculo abdominal (Sección 3.1). Utilizando los datos experimentales y realizando un ajuste numérico se han obtenido un conjunto de parámetros, para la función densidad de energía planteada, que son capaces de reproducir el comportamiento mediante un modelo de elementos finitos (FE) (Secciones 3.3 y 3.4). La simulación se realiza considerando el músculo como un material compuesto

y, por otra parte, considerando la unión de dos capas musculares. De esta forma se concluye y verifica que se puede simular el músculo abdominal de las dos formas planteadas, puesto que ambos FE reproducen el ensayo experimental, Figura 4.

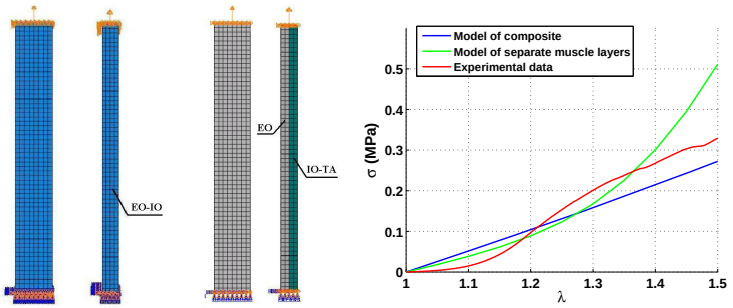

(a) (b) (c)

Figure 4: Modelo de elementos finitos del tejido muscular. Vistas laterales y frontales. (a) Se considera el músculo como un material compuesto (EO-IO). (b) Se considera el modelo considerando el músculo como la unión de dos capas musculares. (c) Curvas obtenidas para los dos modelos planteados y curva experimental de la probeta EO-IO.

Una vez entendido el comportamiento mecánico del músculo abdominal, se realiza la caraterización mecánica de tres mallas quirúrgicas utilizadas en la cirugía abdominal para la reparación herniaria, Surgipro® (SUR), Optilene® (OPT) e Infinit® (INF), Figura 5, mediante ensayos uniaxiales. Se concluye de estos ensayos que la malla Surgipro tiene un comportamiento anisótropo mientras que las mallas Optilene e Infinit presentan un comportamiento anisótropo. A su vez, se compara su comportamiento con el de la pared abdominal, para estudiar qué malla es la que mejor reproduce el comportamiento de la pared abdominal, Figura 6, y concretamente es la malla INF.

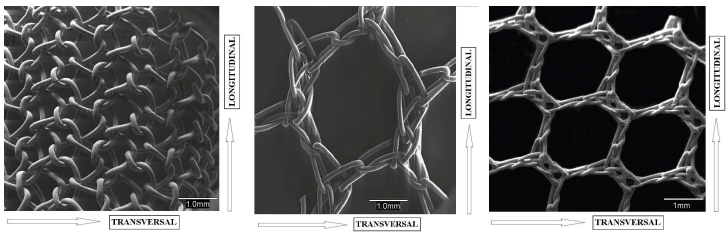

(a) (b) (c)

Figure 5: (a) Malla Surgipro® . (b) Malla Optilene® . (c) Malla Infinit® .

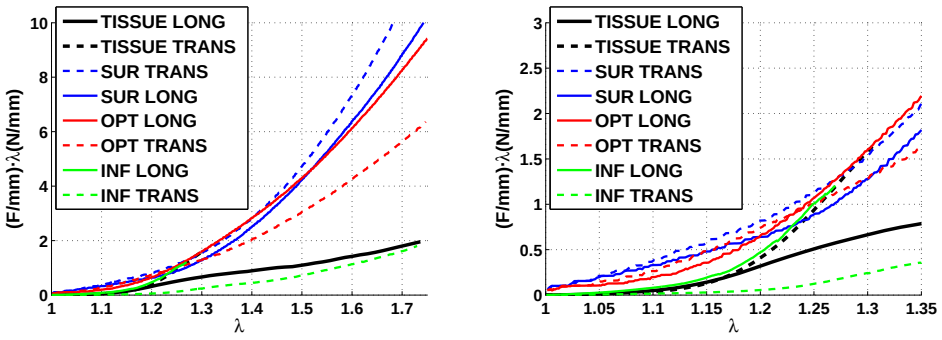

(a) (b)

Figure 6: Tensión de Cauchy equivalente vs. alargamiento para el tejido abdominal y para las mallas estudiadas. Curvas medias experimentales en las direcciones longitudinal y transversal. (a) Gráfica completa. (b) Vista ampliada para bajos alargamientos.

Referido al modelado matemático, se ha definido un modelo constitutivo en 2D para cada una de las mallas (Sección 3.2). En función del comportamiento isótropo o anisótropo, la función densidad de energía elegida es diferente (Sección 3.3). Dentro de este contexto, se realiza un ajuste numérico y se obtienen los parámetros para cada malla que mejor reproducen los ensayos experimentales en ambas direcciones (Sección 3.4). Dicho ajuste se valida mediante un modelo de elementos finitos que reproduce el ensayo experimental de las mallas, Figura 7.

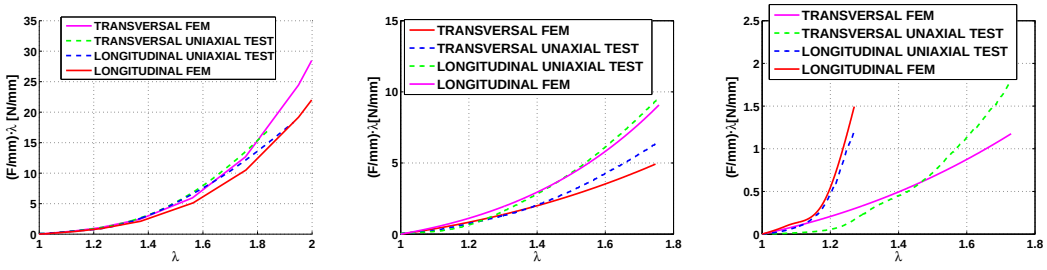

(a) (b) (c)

Figure 7: Tensión de Cauchy equivalente vs. alargamiento para los ensayos uniaxiales, en ambas direcciones; datos experimentales y simulación por elementos finitos. (a) Malla Surgipro® . (b) Malla optilene® . (c) Malla infinit® .

En último lugar, con el objetivo de reproducir el comportamiento del abdomen sin dañar y el abdomen que ha sufrido una cirugía abdominal, se plantea un modelo simplifi-

cado de elementos finitos que simula el abdomen del animal de experimentación utilizado sometido a una presión abdominal interna, Figura 8. Con este modelo se trata de ver cómo se comporta el conjunto del abdomen bajo la presencia de las diferentes mallas estudiadas analizando las tensiones máximas que aparecen (Figura 9) y los desplazamientos máximos producidos (Figura 10).

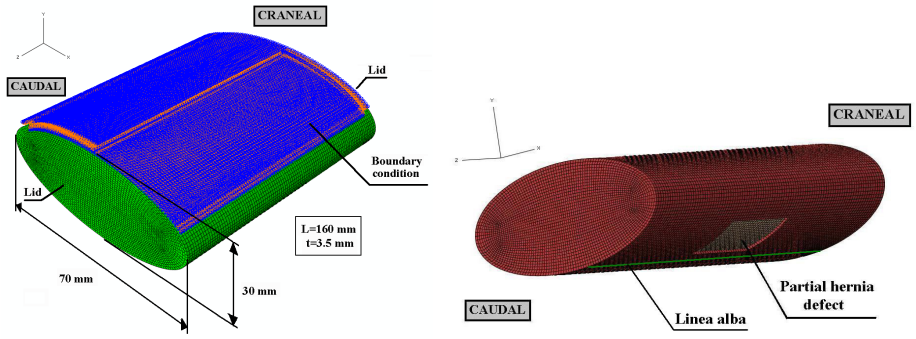

(a) (b)

Figure 8: (a) Modelo simplificado del abdomen del conejo donde la dirección craneo-caudal está indicada, así como las condiciones de contorno. (b) Modelo simplificado del abdomen del conejo, donde hay una hernia parcial.

Puesto que el objetivo que queda por encima de todo es conseguir que el comportamiento de la malla implantada en la pared abdominal pueda reproducir el comportamiento del músculo abdominal sano, el modelo simplificado ayuda a focalizar las deficiencias que se presentan con las mallas actuales. Las tensiones máximas principales alcanzan su máximo valor en la línea de sutura, indicando que en esa zona se produce una concentración de tensiones. Respecto a los desplazamientos, se observa cómo los desplazamientos son menores cuando se tiene una malla implantada, lo cual indica que se está produciendo una restricción en el movimiento del abdomen debido a la presencia de la malla sintética.

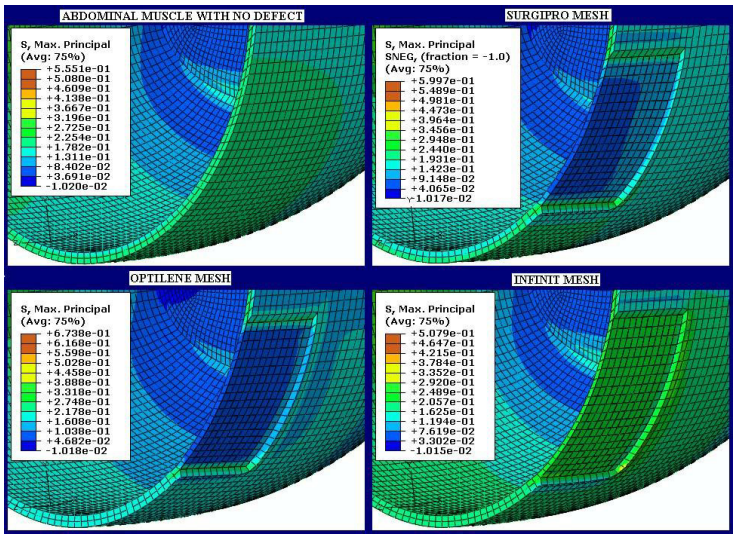

(a)

Figure 9: Tensiones máximas principales en la zona del defecto. Se compara la pared abdominal sana con las diferentes mallas estudiadas.

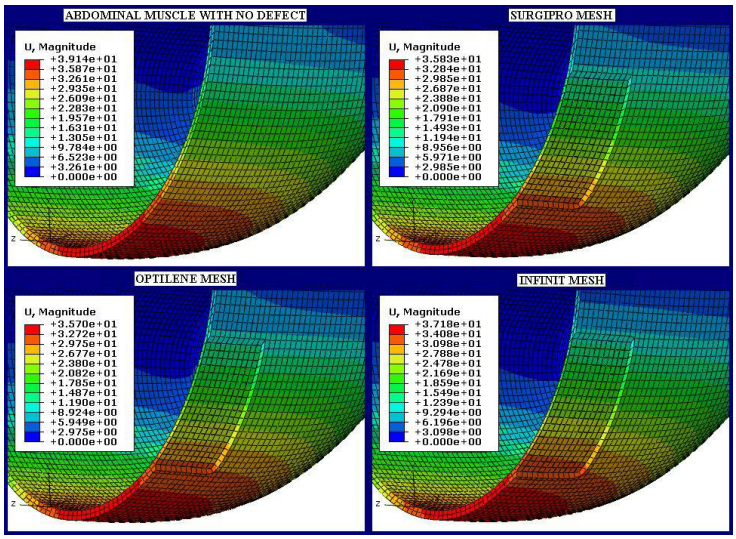

(a)

Figure 10: Desplazamientos máximos en la zona del defecto. Se compara la pared abdominal sana con las diferentes mallas estudiadas.

Contents

Chapter 1

Introduction

1.1 Abdominal muscle

Abdominal muscles contribute to protective reflexes (such as cough, sneeze and vomiting), generate intra-abdominal pressures necessary for expiratory efforts and are active during postural. During inspiration, the diaphragm descends, the abdominal pressure increases, passive abdominal wall tension increases, and the abdominal wall lengthens passively. Contraction of abdominal muscles during expiration causes an inward displacement of the abdominal wall and an increased abdominal pressure, which displaces the diaphragm into the thorax and decreases lung volume [12].

The abdominal wall contains the four most powerful expiratory muscles in mammals: the external oblique (EO), the internal oblique (IO), the transversus abdominis (TA) and the rectus abdominis, Figure 1.1. Anatomically, the IO lies internal to the EO muscle in the lateral abdominal wall, whereas the TA, the most internal abdominal muscle, lies in the lateral and ventral abdominal wall between the internal surface of the IO and the costal cartilage [29].

The EO functions to pull the chest downwards and compress the abdominal cavity, which increases the intra-abdominal pressure. It also has limited actions in both flexion and rotation of the vertebral column.

The IO performs two major functions. First, it acts as an antagonist to the diaphragm, helping to reduce the volume of the thoracic cavity during exhalation. When the diaphragm contracts, it increases the volume of the lungs which then fill with air. Conversely, when the IO contracts it reduces the volume of the air filled lungs, producing an exhalation. Secondly, its contraction rotates and side-bends the trunk by pulling the rib cage and midline towards the hip and lower back, of the same side. It acts with the EO muscle of the opposite side to achieve this torsional movement of the trunk. For example,

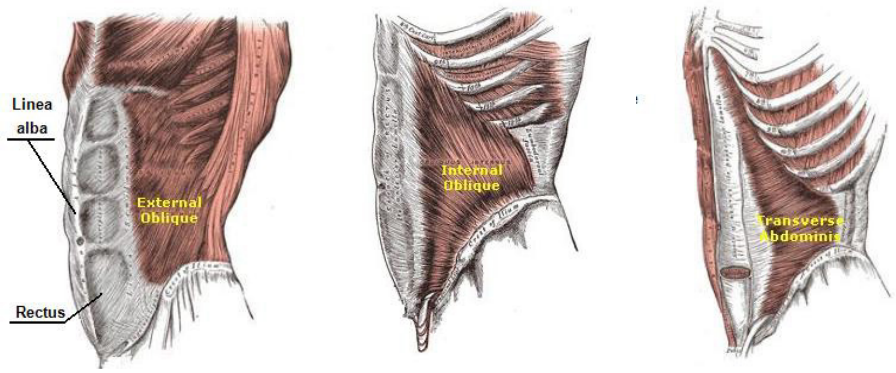

(a) (b) (c)

Figure 1.1: Expiratory muscles in mammals. (a) EO and rectus abdominis. Linea alba is remarked. (b) IO. (c) TA.

the right IO and the left EO contract as the torso flexes and rotates to bring the left shoulder towards the right hip.

The TA helps to compress the ribs and visceras, providing thoracic and pelvic stability. The TA also helps pregnant women deliver their child.

The rectus abdominis is responsible for flexing the lumbar spine. The rectus abdominis assists with breathing and plays an important role in respiration. It also helps in keeping the internal organs intact and in creating intra-abdominal pressure, such as when exercising or lifting heavy weights, during forceful defecation or parturition (childbirth).

Regarding the constitutive behaviour of macroscopic material, muscle tissue is usually considered as a network of muscle fibres, collagen and elastin embedded in a more or less isotropic matrix. In this case, it is necessary to distinguish between collagen and muscular fibres because in the muscle tissue, collagen fibres are principally responsible for passive mechanical strength and stiffness while muscle fibres take care of the contraction. For abdominal tissue, the angle between muscular and collagen fibres is different from zero [24, 20, 32]. The direction of collagen fibres are supposed to determine direction of material anisotropy in order to study passive behaviour and develop the corresponding passive constitutive model [2] while muscle fibres have to be considered in active behaviour. The purely passive response of these soft tissues is often modeled within the framework of hyperelasticity mechanics by means of a strain energy function (SEF) expressed in terms of kinematic invariants, as first developed by Spencer [42]. Muscle tissue, in addition, has the unique characteristic of generating forces through fibre contraction. In this case, it is common to describe the material behaviour as the addition of both passive and active contributions in the SEF [27, 14, 5, 43].

1.2 Abdominal hernia. Surgical meshes

A hernia is an abnormal protrusion of part of an organ through the tissues that normally contain it. In this condition, an opening or weakness in the muscular structure of the wall of the abdomen allows part of the organ to protrude, Figure 1.2. Hernias cause pain and reduce general mobility. They never cure themselves, even though some can be cured by external manual manipulation. Depending on the nature of the protruding organ and the solidity of the structure through which it is protruding, a hernia may cause complications that are medically dangerous.

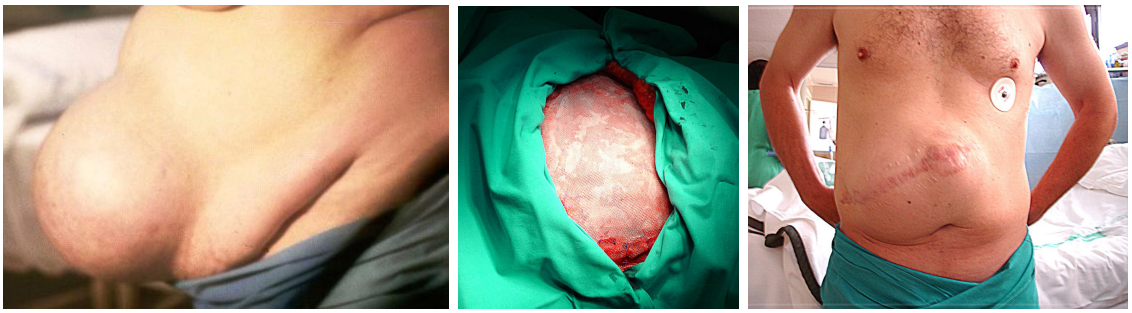

(a) (b) (c)

Figure 1.2: (a) Example of an abdominal hernia defect. (b) Abdominal surgery of hernia repair by implantation of a synthetic mesh. (c) Healed hernia in (a).

A hernia may develop in almost any part of the body. However, the muscles of the abdominal wall are most commonly affected. Technically, this group also includes inguinal hernias and umbilical hernias. The other types of hernias are umbilical hernia, incisional hernia and hiatal hernia between others. Another classification of hernias indicates that there are total hernias or partial hernias. When a total hernia appears all the muscle layers have been opened. On the other hand, a partial hernia appears when a single layer has been opened, and usually, EO failures. Nowadays, partial abdominal hernia is the most common hernia.

Referring to treatment of hernia, for small hernias, various supports may offer temporary, symptomatic relief. However, the best treatment is herniorrhaphy (surgical closure or repair of the muscle wall through which the hernia protrudes). When the weakened area is very large, some biomaterial may be sewn over the defect to reinforce the weak area. Postoperative care involves protecting the patient from respiratory infections that might cause coughing or sneezing, which would strain the suture line.

Thus, hernia repair by implantation of synthetic meshes is the gold standard in this type of abdominal surgery. In technical terms, the repair of a hernia defect in the abdom-

inal wall using a biomaterial has become routine clinical practice. Nowadays, 2.000.000 meshes are being implanted in the developed world and abdominal surgery is the second type of non-emergency surgery in the United States. However, despite the use of prosthetic materials for the repair of abdominal wall defects, hernia recurrences still occur as well as other problems such as inflammatory reactions or adhesions between the implanted material and organs [39, 40].

Nowadays, different types of surgical meshes exist and they can be classified depending on their geometric structure (determines the isotropic or anisotropic behaviour), the material composition (determines the compliance) and the porosity (determines the remodelling and growth of the tissue). Regarding to the geometry and the weave of the filaments, reticular meshes, laminar meshes and composed meshes exist, Figures 1.3, 1.4 and 1.5, respectively. The material of the meshes can be polypropilene, ePTFE, silicona and polyurethane between others, Figures 1.3, 1.4 and 1.5. According to the porosity [8], depending on the weight per surface area expressed as g/m^2, prosthesis may be classified into the classic heavyweights (HW) whether their density is above of 80 g/m^2 and into lightweight (LW) whether their density is below of 50 g/m^2. A third type or mid-weight prosthesis with a density between 50 and 80 g/m^2 is known as mediumweight (MW).

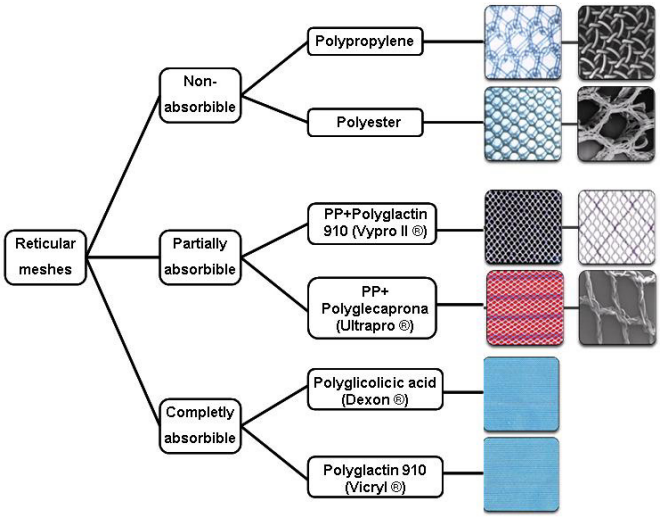

Figure 1.3: Classification of reticular meshes.

Due to the great variety of meshes available on the market worldwide, surgeons have difficulty in choosing the ideal prosthesis for hernia repair. For tissue repair, polypropylene is still the preferred material [34, 1, 3] as well as reticular prothesis. However, over the years this material has undergone modifications to its structure and porosity aimed at improving its adaptation to the host tissue. These changes have tried to reduce the foreign

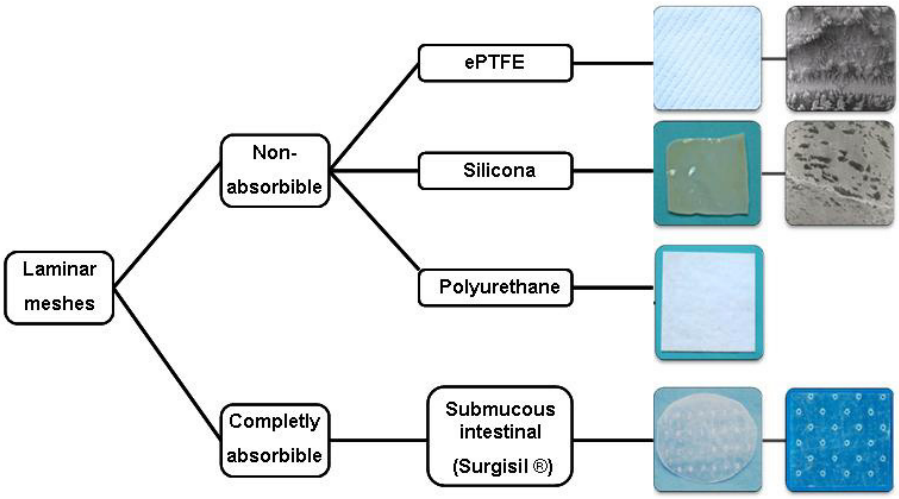

Figure 1.4: Classification of laminar meshes.

body reaction and fibrosis provoked at the implant site. Despite these improvements, the "ideal prothesis" in terms of pore size and spatial structure best adapted to the mechanical conditions of the host tissue has not yet been achieved.

1.3 Objectives

In this context, the final objective is establishing a methodology in order to choose or design the "ideal prothesis", analyzing the results from an experimental animal model and those from a finite element model. Some partial objectives are:

- Passive mechanical characterization of abdominal muscle tissue of the experimental animal (New Zealand White rabbits) through uniaxial tests.

- Mechanical characterization of three surgical meshes (Surgipro®, Optilene® and Infinit®) used in abdominal surgery for hernia repair through uniaxial tests.

- Definition and implementation of a strain energy function (SEF) for the abdominal muscle tissue and for each of the surgical meshes using a UMAT subroutine in Abaqus code in order to carry out a numerical adjustment and obtain the material model parameters.

- Definition of a simplified finite element (FE) model of the abdominal cavity in order to reproduce the mechanical behaviour of the healthy abdominal wall and the abdominal wall after surgery with an implanted mesh.

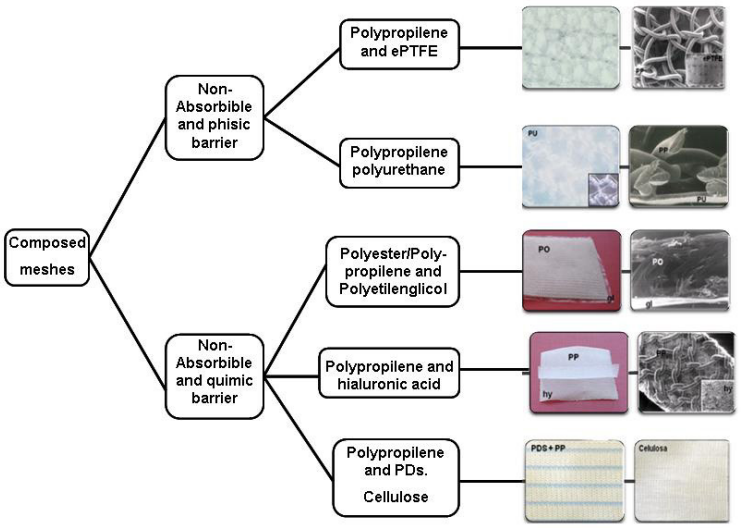

Figure 1.5: Classification of composed meshes.

1.4 Contents

Chapter 1 includes an introduction of the abdominal muscle and surgical meshes used in hernia repair. Next, the objectives of this work are listed and, finally, their contents are described.

Chapter 2 includes the mechanical characterization of the abdominal wall using the New Zealand White rabbit as the animal model. Also, a histological study is included in order to provide a complete study. Both separate muscle layers and the whole muscle are studied separately. On the other hand, a mechanical characterization of three different meshes in two perpendicular directions is included in this Chapter. Finally, a comparison between abdominal wall behaviour and surgical meshes behaviour is presented.

Chapter 3 is referred to the constitutive modelling and it is developed for the 3D and 2D formulations. The strain energy functions used in each case are defined in order to carry out the numerical adjustment of the experimental curves. After that, several groups of constants, the material model parameters, are obtained for each type of material.

Chapter 4 includes different FE models. Two FE models that reproduce the uniaxial test of the abdominal wall and the uniaxial test of the three surgical meshes are presented in order to validate the material model parameters previously obtained. Finally, a simplified FE simulation of the rabbit abdomen is developed in order to reproduce the behaviour of the abdominal cavity. In this case, the whole model as healthy abdominal wall is considered and, on the other hand, a partial hernia is provoked.

Chapter 5 describes some limitations of the study and proposes some future lines of work in order to improve that investigation.

Chapter 2

Experimental characterization

In this chapter, it is presented a systematic study of the *in vitro* passive mechanical characterization of muscle tissue. An in-depth analysis of the mechanical properties of the implant site, in this case the abdominal wall, has been realized. Thus, using the New Zealand White rabbit as a well-known and extensively used animal model [34, 30, 31, 23, 13, 21] the lateral wall of the abdomen have been characterized. In addition, a histological study is included in order to provide a complete characterization of the abdominal wall. Because of the different fibre orientation in each layer of the abdominal wall (collagen and muscular fibres), single layers are analyzed in comparison to the muscle as a whole considered as a composite material. At the same time, it was necessary to know the behaviour of the EO muscle layer due to the fact that partial hernia repair is more frequent in abdominal surgery when only the EO muscle layer is replaced. Furthermore, initial strains are needed to take into account the actual initial configuration and associated strain and stress distributions. Thus, initial strains have been studied.

Referring to the study of the clinical effect of the meshes, a complete and mechanical characterization of the meshes in two perpendicular directions is realized since pore size and spatial arrangement provoke isotropic or anisotropic response of the mesh. The vital importance of the consideration of the anisotropy of the mesh is directly related to the *in vivo* behaviour of the muscle tissue once the mesh is implanted, due to the fact that the whole behaviour (tissue and mesh) must reproduce the healthy tissue.

Due to the fact that for good clinical results in abdominal hernia surgery, a perfect correspondence is required between the mechanical properties of the abdominal wall and the mechanical properties of the biomaterial used for repair, a comparison between abdominal muscle tissue and synthetic meshes is presented. This way, some guidelines for surgeons are established in order to determine the best orientation of each mesh.

2.1 Abdominal muscle tissue

2.1.1 Experimental data

As a previous step to studying human behavior, experimental tests have been developed by means of experimental animal models. Specifically, rabbits have been tested [34, 30, 31, 4]. Seven male, New Zealand White rabbits were acclimatized to the experimental laboratories (609/86/CEE ETS 123). The animals were maintained in a temperature controlled room ($22 \pm 1°C$) with 12 hour light-dark cycles with free access to water and food according to European Union guidelines for animal care (EEC 28871-22A9). The body weight of the rabbits was $2150 \pm 50g$. The animals were sacrificed by an intravenous injection of sodium pentobarbital (300 mg/kg) and immediately afterwards, each animal was placed on its back and the abdominal wall and the skin were dissected, along the midline, free circumferentially, Figures 2.1 and 2.2.a.

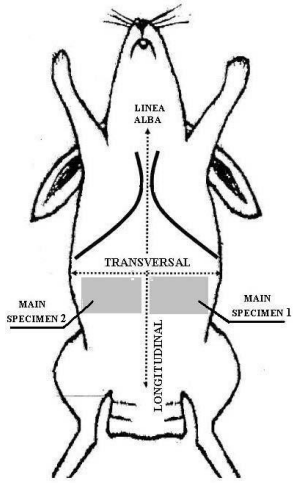

Figure 2.1: Definitions of longitudinal and transversal directions in the rabbit.

2.1.2 Muscle specimen obtaining

Specimens from all the rabbits were taken from the anterior abdominal wall of the animals, Figure 2.2.a. The procedure was carried out making marks in the abdominal wall of the rabbit using a template of $60x100\ mm$ to minimize size variability between the specimens, Figure 2.1, positioning the 60 mm side of the template parallel to the craneo-caudal axis of the rabbit. The specimens were cut from both sides of the rectus abdominis, immediately next to the line where the rectus abdominis finishes, Figure 2.1. Finally, two rectus abdominis tissues were also dissected.

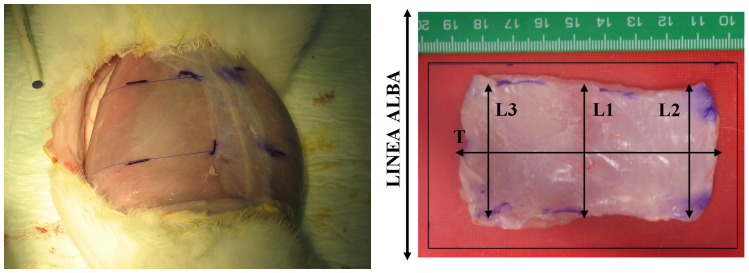

(a) (b)

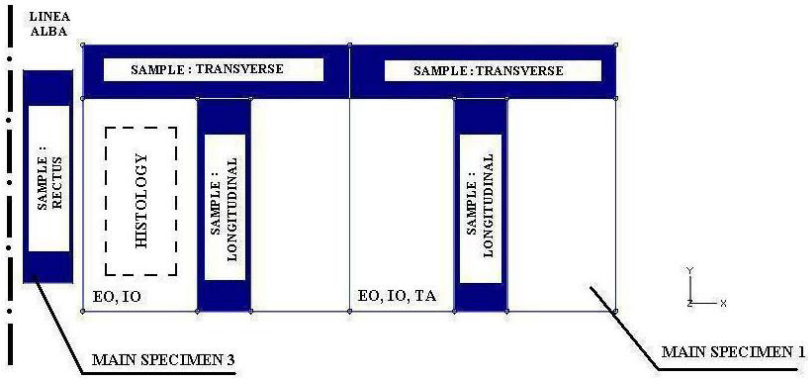

(c)

Figure 2.2: (a) Marks in the anterior abdominal wall of the animals using a $60x100\ mm$ template. (b) Specimen obtained after retraction. (c) The $60x100\ mm$ specimen was sectioned into four samples for tensile testing. The main specimen 2 is placed in the same area but at the left side of the linea alba. Samples for the histologies were obtained from the area included within the dotted line.

2.1.3 Initial strains

Biological soft tissues are usually exposed to a complex distribution of *in vivo* initial strains. This is a consequence of the continuous growth, remodelling, damage and viscoplastic strains that suffer these living materials throughout their whole lives. The real strain distribution of the specimen is three-dimensional and heterogenous and direct measures are very complex. Due to the non-linear behaviour of this tissue, an erroneous inclusion of the initial strain state in computational models can lead to large errors [36]. Therefore the study of muscle retraction was the first step in this study. In this case, shortening of the tissue along different directions was measured to estimate these initial strains. For the sake of clarity, longitudinal direction is here defined as the cranial to caudal

direction of the rabbit, while the transversal corresponds to the perpendicular direction, Figure 2.1.

Prior to cutting each specimen, the shortening of the tissue in two directions is evaluated, longitudinal (L1, L2 and L3) and transversal (T), Figure 2.2.b. Two zones can be differentiated in the specimen studied, one half composed of two muscles (the IO and the EO) and close to the rectus abdominis and the linea alba and the other half comprising three muscles (the IO, the EO and the TA) and close to the para-spinous muscle, Figure 2.2.b. The retraction was measured 15 minutes after the rabbit was sacrificed and the specimen extracted, in order to avoid viscoelastic effects and to preserve the mechanical properties of the tissue. This retraction was measured by means of changes in the distances between pixels in photographs. The muscle shape of the specimen remained approximately rectangular which indicates that the specimen has been taken more or less along its principal material axes. The results of the shortening, Figure 2.2.b, are presented in Table 2.1.

	$Retraction - L1(\%)$	$Retraction - L2(\%)$	$Retraction - L3(\%)$	$Retraction - T\ (\%)$
Specimen 1	12.9	28.2	14.5	22.7
Specimen 2	21.5	27.9	12.9	23.4
Specimen 3	18.6	18.7	21.6	28.7
Specimen 4	23.5	22.6	17.9	28.8
Specimen 5	20.5	21.2	11.1	24.0
Specimen 6	24.1	25.9	12.7	16.8
Specimen 7	23.3	25.3	24.6	29.8
Specimen 8	36.3	41.0	34.7	28.1
Mean	22.6	26.4	18.8	25.3
SD	0.0663	0.0676	0.0797	0.044

Table 2.1: Retraction obtained for the abdominal muscle tissue. Mean and SD (standard deviation).

Considering the average, the maximum value of the retraction was 26.4 % in the longitudinal direction (L2), Figure 2.2.b, where the muscle is comprised of three layers. On the other hand, the minimum value was 18.8 %, also in the longitudinal direction (L3) but close to the rectus, Figure 2.2.b, where only two muscles form the tissue.

2.1.4 Muscle samples preparation

After contraction, the specimens were immersed in a saline solution at $4°C$ in order to prevent them drying out. As previously mentioned, two zones can be differentiated in the specimens studied, approximately one half composed of two muscles (EO and IO) and the other one comprising three muscles (EO, IO and TA). In total, six specimens of composite muscle, six separated specimens (EO muscle layer and IO-TA muscle bilayer) and ten samples of the rectus were obtained. During the separation operation, the EO tissue was dissected free from the internal abdominal wall. This way, it was possible to analyze the whole and the individual muscle behaviour.

From each of the specimens described, new smaller samples were extracted, all of them with a width-length ratio of approximately 1:6 or 1:7 in order to preserve the uniaxial hypothesis during the mechanical test. From each half of each specimen two smaller samples were extracted, one in transversal and one in longitudinal direction. The same procedure was done with the other half specimen, Figure 2.2.c, for each rabbit. Specimens with holds, cuts or apparent damage were not tested. A total of 11 samples of EO-IO composite, 9 of EO-IO-TA composite, 12 of EO muscle layer, 11 of IO-TA muscle bilayer and 10 of rectus abdominis were finally tested.

Tissue	Sample	Length (mm)	Width (mm)	CSA (mm^2)	Thickness (mm)	Density (mg/mm^3)
EO-IO	LONG	44.535 ± 10.557	7.925 ± 0.219	24.633 ± 5.425	3.100 ± 0.599	1.08 ± 0.115
	TRANS	40.195 ± 3.670	9.470 ± 0.325	28.513 ± 6.983	3.025 ± 0.841	
EO-IO-TA	LONG	33.565 ± 1.534	8.855 ± 0.007	36.761 ± 8.595	4.151 ± 0.967	1.296 ± 0.419
	TRANS	35.890 ± 4.525	8.205 ± 0.318	33.281 ± 3.968	4.069 ± 0.641	
EO	LONG	36.435 ± 3.756	6.755 ± 0.851	10.930 ± 1.382	1.635 ± 0.280	0.998 ± 0.153
	TRANS	42.935 ± 0.599	7.198 ± 1.526	12.487 ± 1.046	1.770 ± 0.234	
IO-TA	LONG	39.31 ± 4.645	7.090 ± 1.133	15.41303 ± 2.676	2.175 ± 0.123	1.007 ± 0.133
	TRANS	32.092 ± 4.974	7.485 ± 0.518	17.8265 ± 1.139	2.383 ± 0.082	
RECTUS	LONG	44.312 ± 3.652	7.680 ± 1.304	18.9235 ± 3.139	2.495 ± 0.472	0.992 ± 0.147

Table 2.2: Average dimensions of studied specimens (mean ± standard deviation).

For each sample, the total length, width and thickness were measured using a digital caliber. Volume was measured by means of a tube-test, considering the difference between the final and the initial volume. The weight was measured with a balance. The cross-sectional area of the muscle was determined by dividing the muscle mass m by the product of the length L and the density ρ of the muscle $\left(CSA(mm^2) = \frac{m(mg)}{L(mm)\cdot\rho(mg/mm^3)}\right)$. See Table 2.2 for a summary of the measured magnitudes.

2.1.5 Histologies

The tissue remaining in the abdominal wall after harvesting the samples for the mechanical tests (white areas in Figure 2.2.c) was used for the histological studies. A total of seven animals were used in this study. Specimens of the abdominal wall were fragmented into small pieces and oriented longitudinally to the anatomical plane of the animal for the different analyses. This part of the study was developed and provided by the Faculty of Medicine, University of Alcalá, during the research stay working with them.

In order to analyze the orientation of the muscle fibres of the abdominal wall and localization of the collagen fascias light microscopy was used. The samples were fixed in Bouin's solution, embedded in paraffin and cut into 5-μm sections. Once cut the sections were stained with Masson's trichrome (Goldner-Gabe) and examined under the light microscope (Zeiss Axiophot, Carl Zeiss, Oberkochen, Germany). This section stained

with Masson's trichrome localization of the different collagen fascias was observed in green in the subcutaneous and peritoneal sides, and also between the two muscular layers of the abdominal wall, Figure 2.3.a. Light microscopy allowed us to observe the orientation of the muscle fibres. In sections made in the longitudinal anatomical plane in the abdominal wall, the EO muscle layer showed the muscle fibres in an oblique orientation, and the IO muscle layer in a transversal orientation with respect to the longitudinal axis of the animal, Figures 2.3.b and c. These observations allowed us to establish a pattern of arrangement of the muscle fibres of the outer and inner layers of the abdominal wall of rabbits, as shown in Figure 2.4.

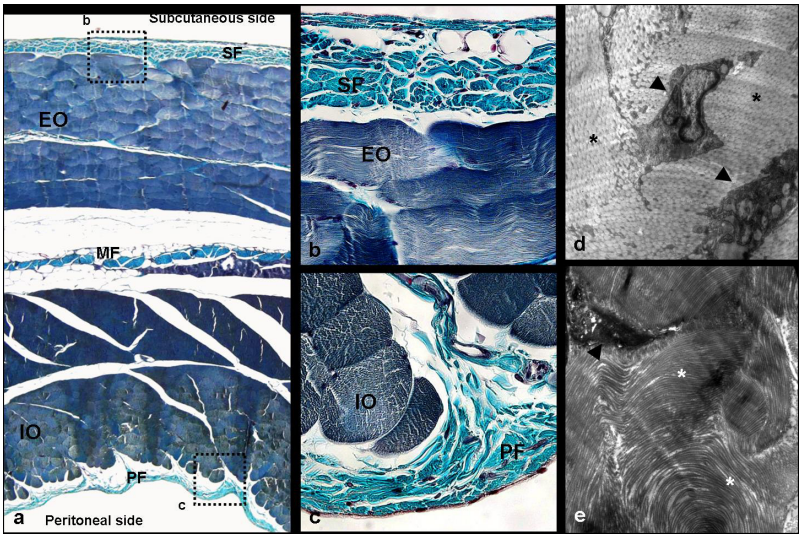

Figure 2.3: a) Panoramic view of a longitudinal section of the abdominal wall of the New Zealand white rabbit. Light microscopy, Masson's trichrome staining, 100X. b) Magnification of the limited area in the dotted square from image a), in the subcutaneous side, showing muscle fibres in oblique disposition in EO muscle layer. Light microscopy Masson's trichrome staining, 400X. c) Magnification of the limited area in the dotted square from image a), in the peritoneal side, showing muscle fibres in transversal disposition in IO muscle layer. Light microscopy Masson's trichrome staining, 400X. d) TEM image of an area from the SF showing collagen fibres in transversal disposition 8000X. e) High magnification of TEM image of an area from the PF showing collagen fibres preferentially arranged in longitudinal disposition. 2500X. (EO: external oblique; IO: internal oblique muscular layers; SF: subcutaneous fascia; PF: peritoneal fascia; MF: medial fascia; Black arrows: fibroblasts; * in black: collagen fibres in transversal section and *in white: in longitudinal section).

In the same sections that were previously used, Sirius red staining was used to localize

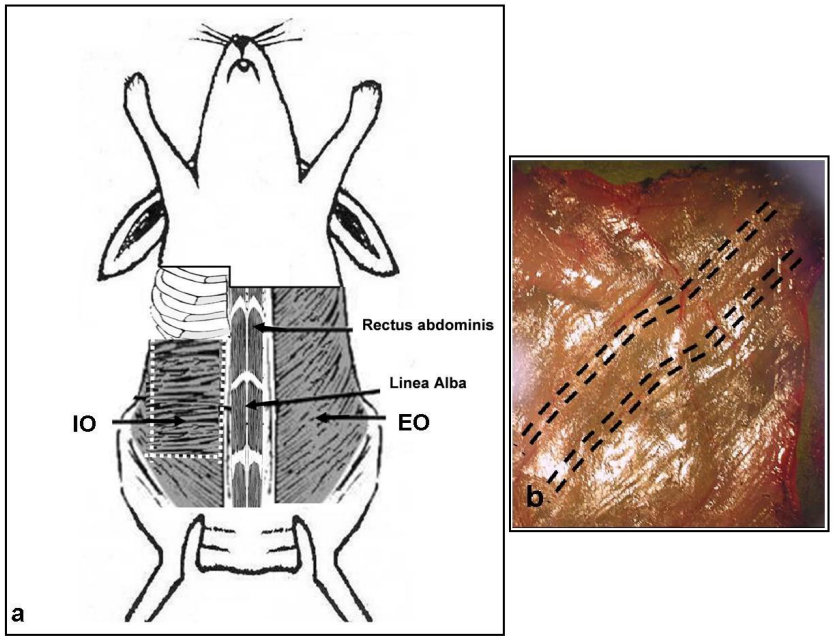

Figure 2.4: a) Model of the arrangement of the skeletal muscle fibres in the abdominal wall of the New Zealand white rabbit (EO: external oblique; IO: internal oblique muscular layers). b) Macroscopic image of the superficial skeletal muscle layer in the left side of the abdominal wall of the experimental animal. The dotted lines represent the direction of the muscle fibres in this area.

and assess collagen types I and III in the abdominal wall. This technique is based on the orientation and interaction between the sulphone groups of the dye, the amine groups of lysin and hydrolysin and the guanidine groups of arginine in the collagen fibres, giving rise to different colours depending on the type of collagen. Collagen type I appears as a reddish-orangey stain while type III collagen takes on a yellow-greenish shade when observed under polarized light microscopy. 10 digitalized histological images per animal were obtained using a digital camera fitted to the microscope (Axiocam HR, Zeiss) and analyzed using image analysis software Axiovision AC 4.1. The percentages of collagens I and III were measured in 5 μm-thick cross sections. This Sirius red staining showed that the different fascias were formed by the mature type of collagen, type I, Figure 2.5. Quantification of the percentage of collagen in the different fascia with respect to the total components of the abdominal wall was analyzed. The subcutaneous fascia represented 11.2 ± 3.9 % of the total components of the abdominal wall, while only 2.5 ± 1.1 % was immature collagen. This fascia was mostly loose, with collagen fibres packed less densely than in the other fascias and sometimes with the presence of adipose tissue in the

highest area. The fascia between the external and the internal muscle layer represented approximately 8.6 ± 4.1 % of collagen I and 0.6 ± 0.3 % of collagen III. The innermost fascia, in the peritoneal side, represented the 7.2 ± 3.3 % collagen I and 0.9 ± 0.4 % collagen type III of the total components of the abdominal wall.

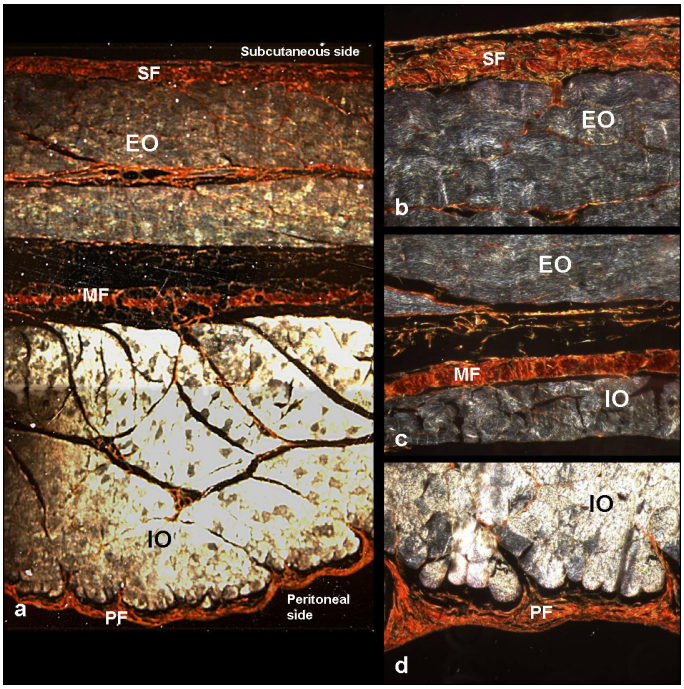

Figure 2.5: a) Image of Sirius red staining showing a panoramic view of a longitudinal section of the abdominal wall of the experimental animals showing that the different fascias are formed by the mature type of collagen (type I). Small amount of collagen type III (in yellow) was observed in the samples. Polarized light microscopy, 100X. b) Magnification of an area in the subcutaneous side, showing the subcutaneous fascia (SF). Polarized light microscopy, 200X. c) Magnification of an area between the outer and inner muscle layers, showing the medial fascia composition (MF). Polarized light microscopy, 200X. d) Magnification of the peritoneal fascia (PF). Polarized light microscopy, 200X. (EO: external oblique; IO: internal oblique muscular layers).

Finally, a ultrastructural study was used to observe the orientation of the collagen fibres in the different collagen fascias. For this analysis, small tissue fragments were fixed for 1 h in 3% glutaraldehyde, stored in Millonig buffer (pH 7.3) and postfixed in 2 % osmium tetroxide. Once dehydrated in a graded series of acetone, the specimens were embedded in Araldite to obtain thin cuts. These sections were counterstained with lead citrate and examined using a Zeiss 109 transmission electron microscope. Analyzing the results in a

longitudinal section, the TEM images showed in the fascial tissue a collagen layer composed of interwoven strands of collagen in different directions, but most of the collagen fibres in the subcutaneous fascia were cross-sectional indicating that they preferentially arranged parallel to the transverse anatomical plane of the animal, Figure 2.3.d. However, in the fascia on the peritoneal side the collagen fibres were preferentially arranged parallel to the longitudinal axis of the animal, Figure 2.3.e.

2.1.6 Mechanical tests

Uniaxial tensile tests were performed under displacement control on an INSTRON 3340 microtester with a 1 kN full scale load cell. Each abdominal muscle sample was preconditioned with three cycles at 40 % or 20 % for the composite muscle or the EO and IO-TA muscle layers, respectively. Slightly higher preconditioning levels were reached compared with the retraction obtained in order to guarantee real working states in all cases. The velocity rate was estimated considering a quasi-static situation. Thus, a velocity rate estimated as 5 mm.min^{-1} was maintained throughout the test and for all specimens. Load and displacement were recorded till complete specimen rupture.

Once load and displacement were recorded, it was possible to obtain stretch data and Cauchy stress. Stretch data is obtained as $\lambda = \frac{L_0+\triangle L}{L_0}$, where L_0 is the initial length between the clamps and $\triangle L$ is the clamp displacement. The Cauchy stress is obtained as $\sigma = \frac{N}{CSA} \cdot \lambda$, where N is the applied load.

In Figures 2.6 and 2.7 the Cauchy stress vs. stretch is represented for the different groups of samples studied. Referring to the EO muscle layer, Figure 2.6.a, the longitudinal direction was less stiff than the transversal, and the rupture stress was also lower in the longitudinal than in the transversal direction. In this case, there is a remarkable anisotropy in the simple muscle behaviour. The IO-TA muscle bilayer had lower failure stress than the EO tissue, Figure 2.6.b. In this case, the longitudinal direction was stiffer with similar rupture stress between the longitudinal and transversal directions, Figure 2.6.b. Figures 2.6.c and 2.6.d show the muscle composite behaviour. For the EO-IO composite, close to the rectus abdominis tissue, the rupture stress was greater than for the EO-IO-TA. No remarkable anisotropy was detected and the results were very similar in the longitudinal and transversal directions. Finally, Figure 2.7. shows the rectus muscle which has a high rupture stress compared with the other areas studied.

In order to analyze the behaviour of the tissue *in-situ*, Cauchy stress vs. stretch divided by the initial stretch is represented for the composite muscle tissue, Figure 2.8. This data includes the passive physiological loading of the tissue by taking into account its initial strains. More remarkable anisotropy of the tissue can be observed when the initial strains are included.

In Figure 2.9.a, the mean curves of the composite and the rectus layer are compared,

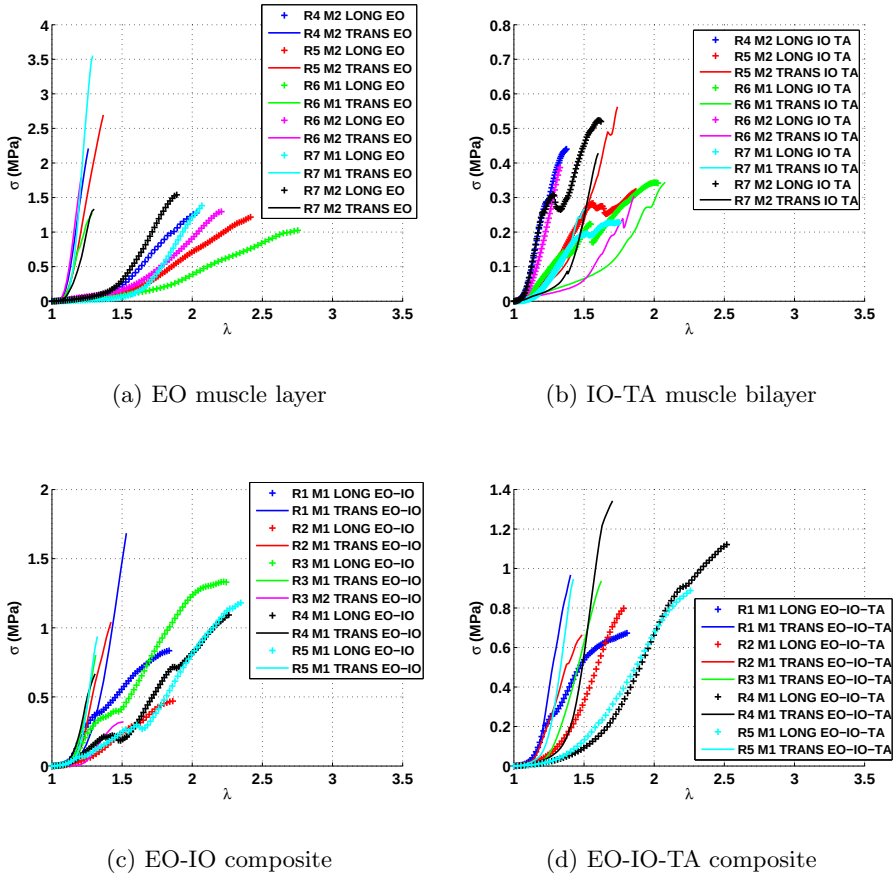

(a) EO muscle layer

(b) IO-TA muscle bilayer

(c) EO-IO composite

(d) EO-IO-TA composite

Figure 2.6: Experimental data of composite muscle layers and separated muscle layers. All experimental curves were truncated before the maximum stress point.

while in Figures 2.9.b and 2.9.c the mean curves for longitudinal and transversal groups of samples, respectively, are represented. The behaviour in the longitudinal direction between the EO-IO and EO-IO-TA is very similar as well as in the transversal direction, Figure 2.9.a. In Figure 2.9.c a remarkable anisotropy is appreciated between the transversal direction for the EO and IO-TA muscle layers while similar results are obtained in the transversal direction when studying the composite. The stiffness in the composite muscle layers and in the transversal direction is an intermediate stiffness between separate muscle layers, Figure 2.9.c. The same fact is observed in Figure 2.9.b but the differences are less pronounced.

As regards to passive behaviour, this study has found that the anisotropic behaviour of the internal abdominal muscles considered as a composite muscle is less pronounced than the individual muscles, Figure 2.9.b and 2.9.c. The transversal direction in the composites

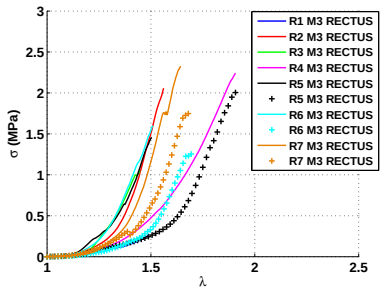

Figure 2.7: Experimental data for rectus sample. All experimental curves were truncated before the maximum stress point.

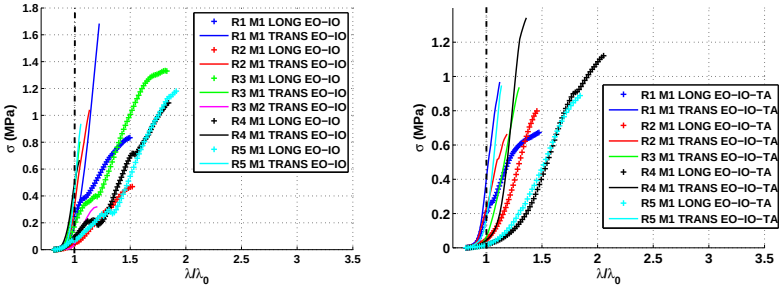

(a) EO-IO composite (b) EO-IO-TA composite

Figure 2.8: Experimental data considering retraction for composite muscle layers. All experimental curves were truncated before the maximum stress point.

is stiffer than the longitudinal direction, Figure 2.9.a. Focussing on the EO muscle layer, the transversal direction is stiffer than the longitudinal, Figure 2.6.a, and this result is related to histological results based on collagen fibre orientation. Fascial tissue in the subcutaneous side is formed preferentially by collagen fibres arranged in the transversal direction, Figure 2.3.b, making this direction stiffer than the perpendicular, Figure 2.6.a. On the other hand, the IO-TA muscle layer is stiffer in the longitudinal direction, Figure 2.6.b, and the results from the histology showed that the inner fascia next to the peritoneal side is formed preferentially by collagen fibres in an oblique arrangement, Figure 2.3.c. The correlation between this fibre arrangement and passive behaviour supports the hypothesis that collagen fibres are responsible for passive mechanical strength and stiffness while muscle fibres take care of the contraction [24, 20, 32, 2]. Focussing on the collagen content, Figure 2.5, the subcutaneous fascia has the greater quantity of collagen and this can

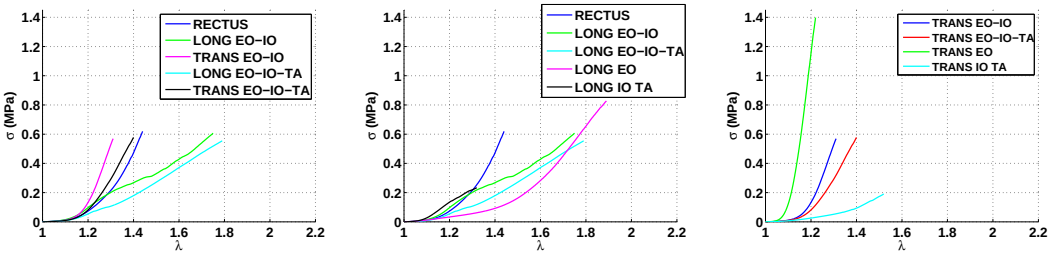

(a) Composites and rectus layer.

(b) Longitudinal samples and rectus layer.

(c) Transverse samples.

Figure 2.9: Mean curves for each group of muscle samples.

explain why the EO muscle layer has a higher rupture stress than the IO-TA muscle layer. Besides, when dissecting the EO free from the internal abdominal wall the fascia between the muscle layers may remain with the EO muscle layer.

2.2 Surgical meshes

2.2.1 Experimental data

Three commercial, elastic, non-absorbible and biocompatible meshes with different pore size and spatial arrangement has been studied. All of them are inert and sterile. Surgipro® (SUR) mesh is a heavyweight (HW) mesh (84 g/m^2) with a small pore size and it is composed of polypropylene monofilament fibres. Optilene® (OPT) mesh is also composed of polypropylene monofilament fibres but, on the contrary, is a lightweight (LW) mesh (48 g/m^2) with a large pore size. Both are indicated for the treatment of abdominal and inguinal hernia as well as in tissue reinforcement. Infinit® (INF) mesh is a mediumweight (LW) mesh (70 g/m^2) with a large pore size and it is composed of PTFE monofilament fibres. In this case, the treatment of hernia repair and defects in soft tissues are indicated. The meshes weaves as well as the two studied directions are shown in Figure 2.10.

2.2.2 Muscle samples preparation

From each mesh, some specimens were cut in longitudinal and transversal direction, Figure 2.10. Rectangular samples with 20 mm of width and 190 mm of length were obtained and the mean value of the thickness was approximately 1 mm, Figure 2.11.a. The number of samples in each direction for the different meshes are shown in Table 2.3.

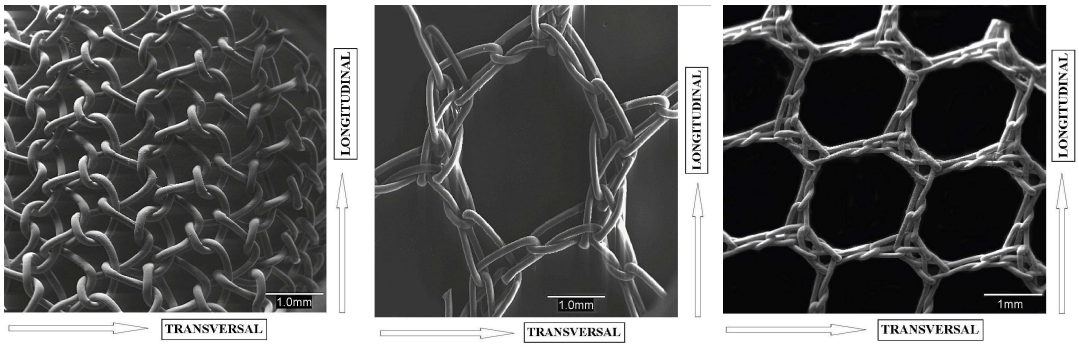

(a) (b) (c)

Figure 2.10: Details of the three meshes, showing both, longitudinal and transversal directions.(a) Surgipro® mesh. (b) Optilene® mesh. (c) Infinit® mesh.

	Longitudinal	Transversal
Surgipro®	3	3
Optilene®	5	5
Infinit®	9	8

Table 2.3: Number of samples in each direction for SUR, OPT and INF meshes.

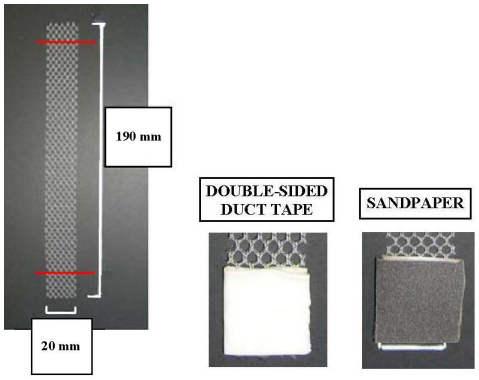

(a) (b)

Figure 2.11: (a) Rectangular sample. Total dimensions: $20x190mm$. Length between clamps: $160mm$. (b) Improved contact in the clamps with double-sided duct tape and sandpaper.

2.2.3 Mechanical tests

The samples were immersed in a Hanks solution during 24 hours. Uniaxial tensile test were performed in an INSTRON 5548 microtester with a 50 N load cell. The contact between the sample and the clamps was improved by means of a double-sided duct tape and sandpaper, Figure 2.11.b, and a free distance between clamps of 160 mm was maintained. Previous to the uniaxial test, a preload of 2 N was applied to each sample and, after that, a displacement rate of 5 mm.min^{-1} was maintained until the rupture of the sample. Stretch data was computed as $\lambda = \frac{L_0+\triangle L}{L_0}$, where L_0 is the initial length between clamps and $\triangle L$ is the displacement. In order to compare the three meshes, force per unit width multiplied by stretch (Equivalent Cauchy Stress, ECS) was obtained using the expression $\frac{Force(N)}{Width(mm)}\lambda$, where Force(N) is the load applied during the test.

Results from mechanical tests are presented for each mesh. In Figures 2.12, 2.13 and 2.14 ECS vs. stretch are represented for the different samples tested, SUR, OPT and INF meshes, respectively.

SUR and OPT meshes reach stretches until approximately 1.9 (90%) in both directions. INF mesh has not the same level of stretches in each direction. Tranversal one is more or less similar to the other meshes but in longitudinal directions the stretch reached is around 1.25 (25%).

Regarding to the maximum ECS, there are relevant differences between meshes. SUR is the most stiffness showing similar behaviour between each direction and reaching values around 20 N/mm. For OPT case, the maximum ECS is reduced to the half being the transversal direction less stiff than longitudinal. Finally, the INF presents a remarkable anisotropy due to the ECS is 1.25 N/mm when the stretch is 1.25 (25%) in longitudinal direction, which is stiffer, and for transversal direction the maximum level is 1.75 N/mm when the stretch is 1.75 (75%).

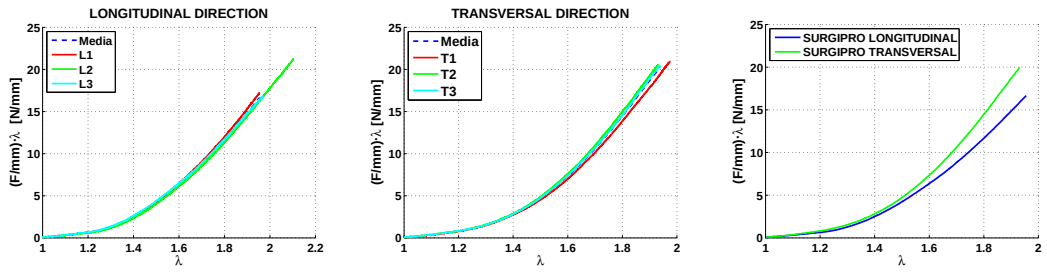

(a) (b) (c)

Figure 2.12: ECS vs. stretch for SUR mesh. (a) Longitudinal direction. (b) Transversal direction. (c) Mean curves in both directions.

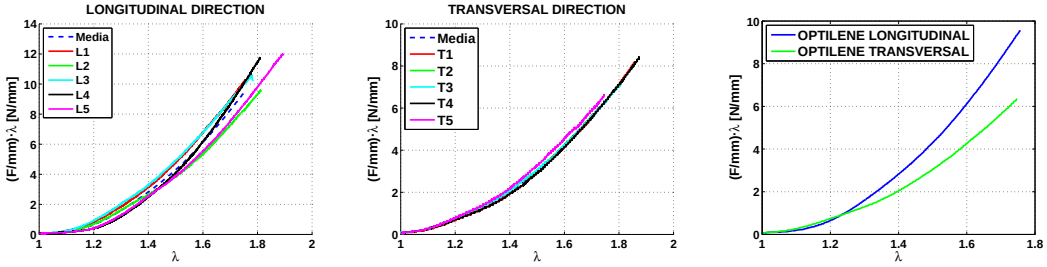

(a) (b) (c)

Figure 2.13: ECS vs. stretch for OPT mesh. (a) Longitudinal direction. (b) Transversal direction. (c) Mean curves in both directions.

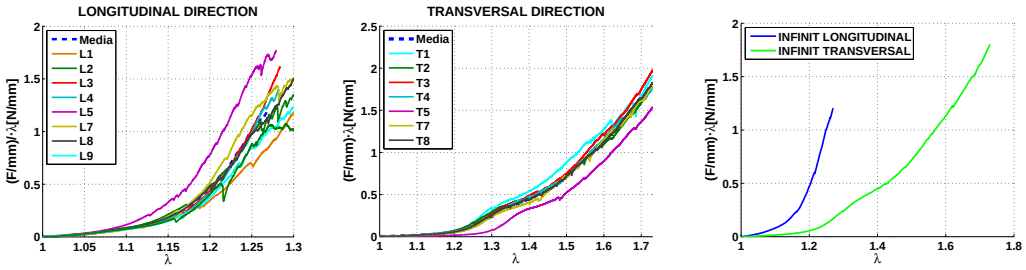

(a) (b) (c)

Figure 2.14: ECS vs. stretch for INF mesh. (a) Longitudinal direction. (b) Transversal direction. (c) Mean curves in both directions.

Analyzing the results, the experimental data presented in this work show that SUR mesh presents an isotropic mechanic response while OPT and INF meshes present an anisotropic behaviour. SUR mesh has similar experimental data in both directions, Figure 2.12.c, and it is justified due to the fact that pore size is very small, Figure 2.10.a, and its spacial arrangement of filaments makes a dense weave, a heavyweight mesh, so the mechanical response of this mesh is isotropic. On the contrary, OPT and INF mesh are lightweight surgical meshes. OPT has a less relevant anisotropic behaviour than the INF, Figure 2.13.c and Figure 2.14.c, respectively. The anisotropic response of both meshes is also justified by the spacial arrangement of the filaments because in both cases the group of filaments aligned with the longitudinal direction are higher than in the transversal one, Figure 2.10.b and 2.10.c. In fact, the mechanical behaviour along the direction of that group of filaments is stiffer than in the other one. So both, OPT and INF meshes are

stiffer in longitudinal direction than in transversal one. Taking into account the level of rupture of the samples, SUR mesh reaches the highest levels, approximately double than OPT one and INF mesh has a very low level of failure compared with the two other ones. The direction of anisotropy obtained for OPT and INF meshes are approximately equal to 0^o, Table 3.3, and that means that longitudinal direction is much stiffer than the other one, that is to say, the behaviour between directions is transversal isotropic. Consequently, in order to establish the good correspondence between abdominal muscle and the surgical meshes, the stiffer direction of the surgical mesh, Figure 2.10, must be disposed in the transversal direction of the abdomen, Figure 2.1. So both, OPT and INF meshes should be disposed in the opposite direction.

2.3 Abdominal muscle tissue vs. Surgical meshes

For good clinical results in abdominal hernia surgery, a perfect correspondence is required between the mechanical properties of the abdominal wall and the mechanical properties of the biomaterial used for repair [9]. The mechanical properties of the abdominal wall were completely characterized, Section 2.1, and Section 2.2 includes a deep study of three kind of surgical meshes. As it has been mentioned, in addition to the material of the filaments, the weave of each mesh, and consequently the spatial arrangement, as well as the pore size determine the mechanical behaviour, the isotropy or anisotropy of the mesh. This issue is a fundamental subject due to the fact that the behaviour of the abdominal wall must be correlated with mechanical behaviour of the mesh in the considered direction.

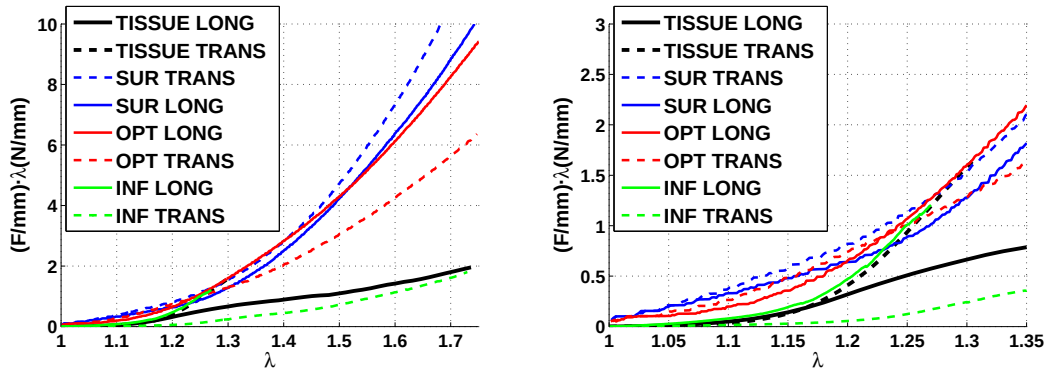

Figure 2.15: ECS vs. stretch for healthy tissue and SUR, OPT and INF meshes. Experimental mean curves from longitudinal and transversal directions. (a) Complete graphic. (b) Zoom view at low stretches.

This way, the comparison between abdominal muscle tissue (EO-IO) and the different kind of studied meshes are presented in Figure 2.15 where experimental data of EO-IO was represented using ECS instead of Cauchy stress. The dotted lines show experimental mean curves in transversal direction and the continue lines shows the longitudinal ones. As a remark, rupture level of each curve is not a vital issue since failure level of meshes reaches higher ranges than abdominal muscle tissue so in Figure 2.15 curves of SUR and OPT were truncated in order to appreciate all the curves. On the contrary, stiffness deserves special attention due to the importance of having similar mechanical response at the level of physiological loads.

Referring to longitudinal direction of muscle tissue, only transversal mean curve of INF mesh has a similar behaviour and the response of the rest of the samples are far from it, Figure 2.15. On the other hand, transversal direction of abdominal muscle tissue behaves in the same way than longitudinal mean curve of INF mesh, Figure 2.15. Besides, the longitudinal and transversal response of SUR and OPT meshes until stretches of 1.3 are lightly stiffer but very similar to transversal direction of healthy muscle tissue, Figure 2.15. In fact, the mechanical behaviour in both directions of SUR and OPT meshes are practically the same at lower values than 1.35, Figure 2.15. As a conclusion and as it has been previously mentioned, INF mesh is the one that best fit the mechanical behaviour of abdominal muscle tissue, but it should be disposed in the opposite direction.

Chapter 3

Constitutive modelling of anisotropic material

In the context of mathematical modelling and finite element (FE) simulation, the experimental data are used to estimate the material model parameters through a strain energy function (SEF) within the framework of the continuum theory of large deformation hyperelasticity. The experimental data showed several relevant features of the muscle tissue and the surgical meshes that should be considered in order to mathematically model the tissue behaviour, Figures 2.6, 2.12, 2.13, 2.14. Firstly, the specimens experienced finite strains for small loads. Secondly, a strongly marked nonlinearity was found. Thirdly, there is a remarkable anisotropy behaviour in some cases, as in single abdominal muscle layer, being less pronounced in the whole muscle, and in some of the meshes. Thus, a preferential direction of anisotropy is considered, through the angle α referred to the longitudinal direction, Figure 3.1.

3.1 Hyperelastic model

A common way to formulate an elastic constitutive law under isothermal conditions for fibred soft tissues, [44, 18, 37], is to postulate the existence of a SEF that depends on the direction of the family of fibres at a point $\mathbf{X}$ that is defined by the unit vector field $\mathbf{m}_0$ [42]. The stretch λ_m of the fibres defined as the ratio between its lengths at the deformed and reference configurations is:

$$\lambda_m^2 = \mathbf{m}_0 \cdot \mathbf{C}\mathbf{m}_0 \tag{3.1}$$

where $\mathbf{F} = \frac{\partial \mathbf{x}}{\partial \mathbf{X}}$ and $\mathbf{C} = \mathbf{F}^T\mathbf{F}$ are the standard deformation gradient and the corresponding right Cauchy-Green strain measure, respectively.

In order to describe the current deformation state and taking into account initial

strains, the methodology proposed by Gardiner and Weiss [15] is followed to enforce initial strains in hyperelastic soft tissues. Three different configurations were defined: a) the stress free state (Ω_{sf}), b) the reference state in which the material is only under the initial strain (Ω_0) and c) the current deformed state (Ω). It was assumed that the total deformation gradient tensor corresponding to the current state $\mathbf{F}$ admits a multiplicative decomposition $\mathbf{F} = \mathbf{F}_r\mathbf{F}_0$, where, $\mathbf{F}_0$ represents the deformation gradient corresponding to the initial strains and $\mathbf{F}_r$ is the deformation gradient that results from applying the external loads to this initial configuration Ω_0.

In order to handle more easily the quasi-incompressibility constraint, a multiplicative decomposition of $\mathbf{F} = J^{\frac{1}{3}}\bar{\mathbf{F}}$ and $\mathbf{C} = J^{\frac{2}{3}}\bar{\mathbf{C}}$ into volume-changing and volume-preserving parts is usually established, as in Simo and Taylor [41], where J is the Jacobian.

To characterize isothermal processes, it is postulated the existence of a unique decoupled representation of the strain-energy density function Ψ:

$$\Psi(\mathbf{C}, \mathbf{M}, \mathbf{N}) = \Psi_{vol}(J) + \bar{\Psi}(\bar{\mathbf{C}}, \mathbf{M}, \mathbf{N}, \beta) \tag{3.2}$$

Where the second term is decoupled in the passive and active response:

$$\Psi(\mathbf{C}, \mathbf{M}, \mathbf{N}) = \Psi_{vol}(J) + \bar{\Psi}_{passive}(\bar{\mathbf{C}}, \mathbf{M}) + \bar{\Psi}_{active}(\bar{\mathbf{C}}, \mathbf{N}, \beta) \tag{3.3}$$

$$\Psi(\mathbf{C}, \mathbf{M}, \mathbf{N}) = \Psi_{vol}(J) + \bar{\Psi}_{passive}(\bar{I}_1, \bar{I}_2, \bar{I}_4) + \bar{\Psi}_{active}(\bar{I}_6, \beta) \tag{3.4}$$

where $\Psi_{vol}(J)$, $\bar{\Psi}_{passive}$ and $\bar{\Psi}_{active}$ are given scalar-valued functions of J and $\bar{\mathbf{C}}$, $\mathbf{M} = \mathbf{m}_0 \otimes \mathbf{m}_0$ and $\bar{\mathbf{C}}$, $\mathbf{N} = \mathbf{n}_0 \otimes \mathbf{n}_0$, β, respectively, that describe the volumetric and isochoric responses of the material [44, 16]. This isochoric response is also formed by the active and passive response of the material; $\mathbf{M}$ and $\mathbf{N}$ are the preferential direction of anisotropy for the collagen fibers and muscle fibers, respectively, and β is the activation level. $\bar{I}_1$ and $\bar{I}_2$ are the first and second modified strain invariants of the symmetric modified Cauchy-Green tensor $\bar{\mathbf{C}}$. Finally, the invariants $\bar{I}_4 \geq 1$ and $\bar{I}_6 \geq 1$ characterizes the constitutive response of the fibres in the passive and active behaviour, respectively:

$$\bar{I}_4 = \bar{\mathbf{C}} : \mathbf{M} = \bar{\lambda}_m^2 \tag{3.5}$$

$$\bar{I}_6 = \bar{\mathbf{C}} : \mathbf{N} = \bar{\lambda}_n^2 \tag{3.6}$$

The constitutive equation for quasi-compressible hyperelastic materials can be defined from the Clausius-Planck inequality as:

$$\mathbf{S} = 2\frac{\partial \Psi(\mathbf{C}, \mathbf{M}, \mathbf{N}, \beta)}{\partial \mathbf{C}} = \mathbf{S}_{vol} + \bar{\mathbf{S}} = \mathbf{S}_{vol} + \bar{\mathbf{S}}_{passive} + \bar{\mathbf{S}}_{active} \tag{3.7}$$

Again, the second term is decoupled in the passive and active response:

$$\mathbf{S} = Jp\mathbf{C}^{-\mathbf{1}} + 2\frac{\partial\bar{\Psi}_{passive}(\bar{\mathbf{C}},\mathbf{M})}{\partial\mathbf{C}} + 2\frac{\partial\bar{\Psi}_{active}(\bar{\mathbf{C}},\mathbf{N},\beta)}{\partial\mathbf{C}} \tag{3.8}$$

where the second Piola-Kirchhoff stress $\mathbf{S}$ consists of a purely volumetric contribution $\mathbf{S}_{vol}$ and a purely isochoric one $\bar{\mathbf{S}}$; being $p = \frac{d\Psi_{vol}(J)}{dJ}$ the hydrostatic pressure. The Cauchy stress tensor $\boldsymbol{\sigma}$ is $1/J$ times the push-forward of $\mathbf{S}$ ($\boldsymbol{\sigma} = J^{-1}\boldsymbol{\chi}_*(\boldsymbol{S})$) [16].

Knowing the second Piola-Kirchhoff stress $\mathbf{S}$, the elastic tensor $\mathbb{C}$ is defined in the material configuration as follows:

$$\mathbb{C} = 2\frac{\partial\mathbf{S}(\mathbf{C},\mathbf{M},\mathbf{N},\beta)}{\partial\mathbf{C}} \tag{3.9}$$

The elastic tensor $\mathbb{C}$ consists of a purely volumetric contribution and a purely isochoric one which is also formed by the active and passive response [16]:

$$\mathbb{C} = \mathbb{C}_{vol} + \bar{\mathbb{C}} = \mathbb{C}_{vol} + \bar{\mathbb{C}}_{passive} + \bar{\mathbb{C}}_{active} = 2\frac{\partial\mathbf{S}_{vol}}{\partial\mathbf{C}} + 2\frac{\partial\bar{\mathbf{S}}_{passive}}{\partial\mathbf{C}} + 2\frac{\partial\bar{\mathbf{S}}_{active}}{\partial\mathbf{C}} \tag{3.10}$$

The elastic tensor in the spatial configuration, denoted by $_{\mathbb{C}}$, is $1/J$ times the push-forward of $\mathbb{C}$ ($_{\mathbb{C}} = J^{-1}\boldsymbol{\chi}_*(\mathbb{C})$) [16].

3.2 Particularization to membrane model

Due to the fact that the thickness of the meshes are very small, surgical meshes are modeled by means of the membrane model. In that case, stresses in the direction of the thickness have to be zero. This way, constitutive modeling in 3D for anisotropic materials have to be reduced in the membrane model. The method proposed by Klinkel and Govindjee [22] has been followed.

The formulated algorithm is described here as it has been implemented in Abaqus. The code uses a local system of coordinates defined by three vectors. e_1 y e_2 are placed in the membrane plane and e_3 is perpendicular to this plane. These vectors rotate as the rigid solid does and strains are expressed in the local system. The standard deformation gradient $\mathbf{F}$ is expressed as follows:

$$\mathbf{F} = \begin{pmatrix} F_{11} & F_{12} & 0 \\ F_{21} & F_{22} & 0 \\ 0 & 0 & F_{33} \end{pmatrix} \tag{3.11}$$

The C_{33} component of the right Cauchy-Green strain tensor, as well as σ_{33} component, are not null.

In order to start the algorithm, the constitutive 3D law is expressed grouping the second Piola-Kirchhoff stress $\mathbf{S}$ and the elastic tensor $\mathbb{C}$ in null terms ($\mathbf{S}_z = (S_{33}) = 0$) and in not null terms ($\mathbf{S}_m = (S_{11}, S_{22}, S_{12}, S_{13}, S_{23})^T$):

$$\begin{pmatrix} d\mathbf{S}_m \\ d\mathbf{S}_z \end{pmatrix} = \begin{pmatrix} \mathbb{C}_{mm} & \mathbb{C}_{mz} \\ \mathbb{C}_{zm} & \mathbb{C}_{zz} \end{pmatrix} \begin{pmatrix} \mathbf{C}_m \\ \mathbf{C}_z \end{pmatrix} \tag{3.12}$$

Considering equation 3.12, $\mathbf{S}_z = 0$ and $\mathbf{C}_z$ is the unknown component in the deformation gradient. The algorithm is developed by means of a Taylor series:

$$\mathbf{S}_z^{(i+1)} = \mathbf{S}_z^{(i)} + \frac{\partial \mathbf{S}_z^{(i)}}{\partial \mathbf{C}_z^{(i)}} \Delta \mathbf{S}_z + ... \doteq 0 \tag{3.13}$$

Where the superscript i is the number of the local iteration. In the following iterations $\mathbf{C}_z$ is modified until the condition $\mathbf{S}_z = 0$ is reached. Depreciating the high order terms in the Taylor series $\mathbb{C}_{zz}^i = \frac{\partial \mathbf{S}_z^{(i)}}{\partial \mathbf{C}_z^{(i)}}$ is obtained. The incremental deformation is:

$$\Delta \mathbf{C}_z = -[\mathbb{C}_{zz}^i]^{-1} \mathbf{S}_z^{(i)} \tag{3.14}$$

Thus, in the next iteration the deformation is expressed as follows:

$$\mathbf{C}_z^{(i+1)} = \mathbf{C}_z^{(i)} + \Delta \mathbf{C}_z \tag{3.15}$$

The stiffness tangent matrix, used in each iteration in the Newton-Raphson algorithm, should be associated with the variation of $\mathbf{S}_m = 0$ with respect to $\mathbf{C}_m$, but it will depend on the complete deformation state $\mathbf{C}$. In order to obtain the stiffness tangent matrix, considering the imposed stress in the membrane element ($\mathbf{S}_z = (S_{33}) = 0$), it have to be condensed. If $d\mathbf{C} = 0$ in the second equation of 3.13:

$$d\mathbf{C}_z = -\mathbb{C}_{zz}^{-1} \mathbb{C}_{zm} + d\mathbf{C}_m \tag{3.16}$$

Inserting 3.16 in the Ecuation 3.13:

$$d\mathbf{S}_m = \mathbb{C}_{psc} + d\mathbf{C}_m \qquad con \qquad \mathbb{C}_{psc} = [\mathbb{C}_{mm} - \mathbb{C}_{mz} \mathbb{C}_{zz}^{-1} \mathbb{C}_{zm}] \tag{3.17}$$

where $\mathbb{C}_{psc}$ is the stiffness tangent matrix corresponding to the membrane element.

3.3 Strain energy functions

In this section several strain energy functions are proposed for the abdominal muscle tissue and the different meshes.

3.3.1 Abdominal muscle tissue

The isotropic response was modelled by means of Demiray's SEF [11] while the anisotropic response was represented by Holzapfel's SEF [18]:

$$\bar{\Psi} = \bar{\Psi}_{iso} + \bar{\Psi}_{ani} = \frac{c_1}{c_2}(\exp^{\frac{c_2}{2}(\bar{I}_1-3)} - 1) + \frac{c_3}{2c_4}(\exp^{c_4(\bar{I}_4-1)^2} - 1) \tag{3.18}$$

In equation (3.18), $c_1 > 0$ and $c_3 > 0$ are stress-like parameters and $c_2 > 0$ and $c_4 > 0$ are dimensionless parameters (Note: $\bar{\Psi}_{ani} = 0$ if $\bar{I}_4 \leq 1$).

3.3.2 Surgical meshes

Due to isotropic and anisotropic character of SUR and OPT and INF meshes, respectively, the material models used to fit he mechanical response were different.

SUR mesh presents an isotropic behaviour, Section 2.2.3, so the isotropic Yeoh model, which best fits the curves in both, longitudinal and transversal directions, was used. The Yeoh's SEF is the expressed in Equation 3.19, where μ_1 is the shear modulus and $c_{10} > 0$, $c_{20} > 0$ and $c_{30} > 0$ are stress-like parameters. Abaqus code lets do an automatic fit of the curves by means of introducing the results of the experimental test and, automatically, fitted constants are returned by Abaqus. Based on the consideration of an isotropic response, only one mean curve in one direction is needed. Specifically, longitudinal direction has been taken.

$$\begin{aligned} \bar{\Psi} &= \bar{\Psi}_{iso} = c_{10}(\bar{I}_1 - 3) + c_{20}(\bar{I}_1 - 3)^2 + c_{30}(\bar{I}_1 - 3)^3 \\ c_{10} &= \frac{\mu_1}{2} \end{aligned} \tag{3.19}$$

On the other hand, OPT and INF present an anisotropic behaviour. In both cases, the isotropic response was modelled by means of the Demiray's SEF [11] while the anisotropic response was represented by the Holzapfel's SEF [18], Equation 3.18.

In equation (3.18), $c_1 > 0$ and $c_3 > 0$ are stress-like parameters and $c_2 > 0$ and $c_4 > 0$ are dimensionless parameters (Note: $\bar{\Psi}_{ani} = 0$ if $\bar{I}_4 \leq 1$).

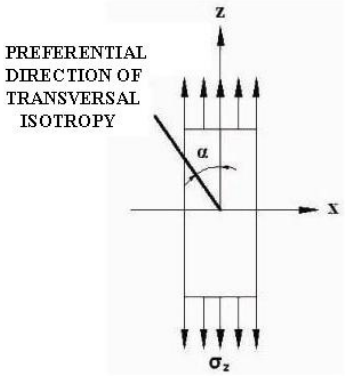

Figure 3.1: Different orientations between uniaxial test in longitudinal direction and the preferential direction of transversal isotropy.

3.4 Model parameters

Fitting of the experimental data was performed using the Levenberg-Marquardt minimization algorithm [26]. This algorithm, widely used for experimental data fitting of soft biological tissues [17], is based upon the minimization of an objective function, which takes the form represented in 3.20 for the uniaxial tension test:

$$\chi^2 = \sum_{i=1}^{n} \left[\left(\sigma^{\exp} - \sigma^{\Psi}\right)_{iL}^2 + \left(\sigma^{\exp} - \sigma^{\Psi}\right)_{iT}^2 \right] \tag{3.20}$$

where $\sigma_i^{\exp}$ and σ_i^{Ψ} represent the measured and the fitted stress values for the ith point data, respectively. The L and T subscript indicates the direction of the test, longitudinal and transversal respectively. The quality of the fittings was evaluated by the normalized mean square root error ε, Eq. 3.21:

$$\varepsilon = \frac{\sqrt{\frac{\chi^2}{n-q}}}{\mu} \tag{3.21}$$

were q is the number of parameters of the SEF, n is the number of data points, $n-q$ is the number of degrees of freedom, and μ is the mean stress defined as $\mu = \frac{1}{n} \sum_{i=1}^{n} [\sigma]_i$.

3.4.1 Abdominal muscle tissue

On the basis of the approach generally adopted in the mechanics of soft tissues, the tissue was assumed as incompressible, that is $I_3 = J^2 = 1$, [33], due to its high water content. Because the collagen fibril orientation is different from the test direction, the classical

uniaxial test is identified by the following deformation gradients in the 3D formulation, Section 3.1: $F_{11} = \lambda_x$, $F_{13} = \kappa$, $F_{22} = (\lambda_x \lambda_z)^{-1}$ and $F_{33} = \lambda_z$ [33]. In this expression, λ_x is the stretch along the x direction, $(\lambda_x \lambda_z)^{-1}$ is the stretch in the y direction, κ is the amount of shear stretch in the xz transversal direction and λ_z is the stretch in the z direction. The latter is known because the test was carried out in the z direction, Figure 3.1.

Due to the complexity of the analytic solution, fitted stress values were obtained by means of a numerical method. Table 3.1 shows the results of the parameter estimation for the muscle tissue including the values obtained for the mean curves simultaneously in longitudinal and transversal directions. In all cases, the very low ε values confirmed the goodness of the fit. In Figure 3.2, the fitted mean curves are shown. Nevertheless, the fitting at low stretch ranges has not a good agreement but this is due to the high exponential character of the curves.

	$c_1(MPa)$	$c_2(-)$	$c_3(MPa)$	$c_4(-)$	$\alpha(^o)$	ε
$EO-IO$	0.16832	0.6319	0.01219	5.68158	87.8	0.17873
$EO-IO-TA$	0.11092	1.12568	0.02568	1.87174	83.6	0.16118
EO	0.06577	1.26785	0.28146	7.02349	88.2	0.17782
$IO-TA$	0.10768	0.11071	0.05814	2.03275	15	0.13871
$RECTUS$	0.03092	3.68821	0.52764	2.07285	21.64	0.07379

Table 3.1: Material parameters of abdominal muscle tissue obtained from the fitting procedure. The angle α is considered between the longitudinal direction and the preferential direction of transversal isotropy

3.4.2 Surgical meshes

Following the 2D formulation, Section 3.2, the constants of the material models for surgical meshes were obtained by means of an iterative process minimizing the error between experimental and fitted curves. The results are shown in Tables 3.2 and 3.3.

	D	$C_{10}(MPa)$	$C_{20}(MPa)$	$C_{30}(MPa)$
$Surgipro$®	0.0	0.48218	0.61706	0.014282

Table 3.2: Material parameters of SUR mesh obtained from the fitting procedure.

	D	$c_1(MPa)$	$c_2(-)$	$c_3(MPa)$	$c_4(-)$	$\alpha(^o)$	ε
$Optilene$®	0.001	1.21065	1.38021	0.2	0.00472	0.0	0.1570
$Infinit$®	0.001	0.3	2.19314	0.01	5.49131	0.0	0.3837

Table 3.3: Material parameters of OPT and INF meshes obtained from the fitting procedure. The angle α is considered between longitudinal direction and the preferential direction of transversal isotropy.

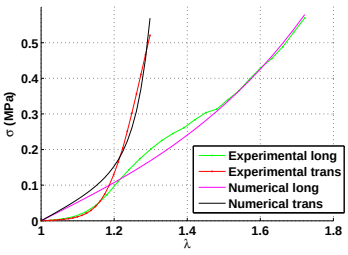

(a) LA-TB area. EO-IO composite

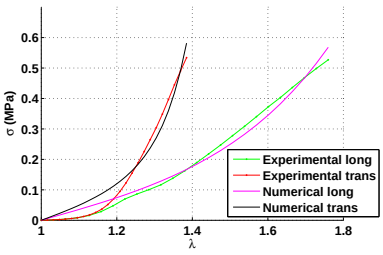

(b) LC-TD area. EO-IO-TA composite

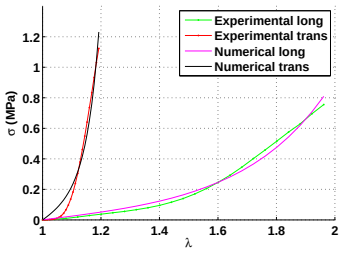

(c) LA-TB area. EO muscle layer

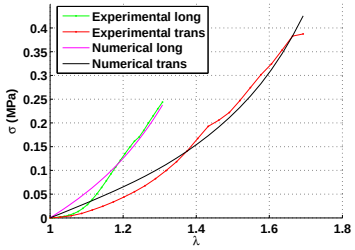

(d) LA-TB area. IO-TA muscle bilayer

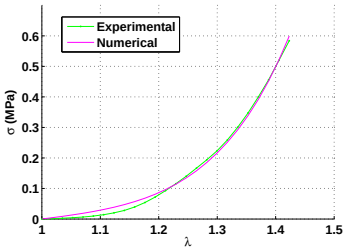

(e) RECTUS area.

Figure 3.2: Experimental *versus* numerical stress-stretch relationships for each muscle specimen.

Chapter 4

FEM Simulation

According to abdominal wall, a methodology is proposed to reproduce the abdominal muscle tissue behaviour by FE simulations using 3D elements. On the other hand, referring to surgical meshes, a methodology is proposed to reproduce their behaviour by FE simulations using membrane elements due to their small thickness. The anisotropic response is modelled by means of the definition of a preferential direction of anisotropy [42]. Abdominal muscle tissue as well as each mesh are modelled through a SEF within the framework of the continuum theory of large deformation hyperelasticity once the material model parameters have been obtained, Section 3.4. After that, experimental and numerical results are compared.

Finally, a FE simulation of a simplified model of the rabbit abdomen is proposed. The whole model as healthy abdominal wall is considered and, on the other hand, a partial hernia is provoked in the abdominal wall. Considering the partial defect, the three different meshes are simulated as they were sewn over the defect. Thus, maximal displacements as well as maximal principal stresses are analyzed. If the maximal displacements, once the mesh has been implanted, are lower than in the healthy abdominal wall that means that the mesh provokes discomfort in the patient. The maximal principal stresses are related to stress state defined by the process of wound healing.

4.1 FEM Simulation of abdominal muscle tissue

In order to prove that the mathematical model can reproduce the behaviour of the tissue, this FE simulation of the experimental uniaxial test was reproduced using a UMAT subroutine in Abaqus commercial code, Figure 4.1. This simulation was carried out considering the sample as a composite in a unique layer, Figure 4.1.a, and, on the other hand, considering the sample as the junction of two muscle layers, Figure 4.1.b. Regarding to the

material, a UMAT subroutine was implemented to incorporate the SEF of muscle tissue, Equation 3.18, and the material parameters were the constants obtained previously in the fitting procedure, Table 3.1.

The FE model was constructed with 2745 nodes and 1920 C3D8H elements of Abaqus commercial code. Boundary conditions simulate the uniaxial test. Displacements are fixed in all directions in the lower clamp. In the upper side a displacement corresponding to a 50% of strain is imposed in the axial direction.

Figure 4.1.c presents the curves corresponding to the FE models and the experimental mean curve obtained in longitudinal direction for the EO-IO sample. In Figure 4.1.c, the three curves are quite similar showing that the assumption of modeling the tissue as a composite or as two separate muscle layers is correct and that the results are acceptable.

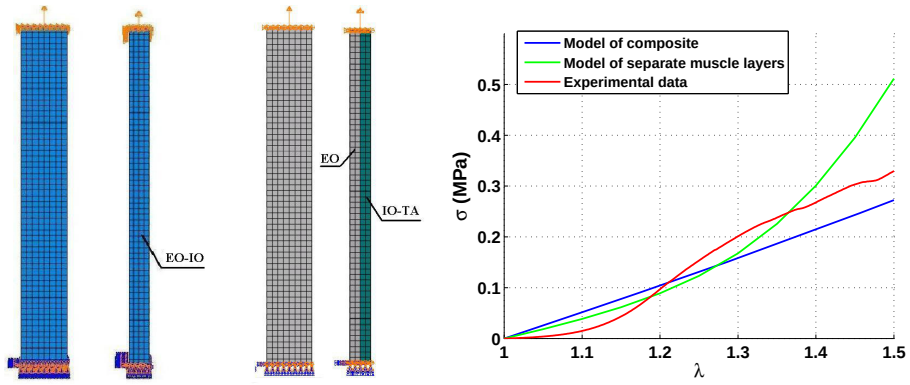

(a) (b) (c)

Figure 4.1: FE model of muscle tissue with C3D8H elements. Boundary conditions in lower clamp and applied load in upper clamp are indicated. (a) Front and lateral view of the FE simulation of the model of the tissue as a composite (EO-IO). Angle $\alpha_{EO-IO} = 87.8^{o}$, Figure 3.1. (b) Front and lateral view of the FE simulation of the model of the tissue using separate muscle layers. Angle $\alpha_{EO} = 88.2^{o}$ and angle $\alpha_{IO-TA} = 15^{o}$, Figure 3.1. (c) Obtained curves considering two models, separate muscle layers and composite, and curve of experimental longitudinal EO-IO sample.

4.2 FEM Simulation of meshes

Due to the fact that the thickness of the surgical meshes is very small, the FE model was constructed with 165 nodes and 128 M3D4 membrane elements of Abaqus commercial code. Regarding to the material, a UMAT subroutine was implemented to incorporate the SEF of OPT and INF meshes, Equation 3.18, and a material of the library was used for

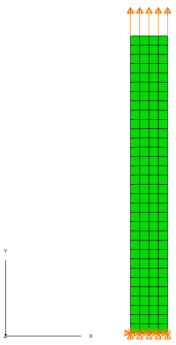

Figure 4.2: FE model of meshes with M3D4 elements. Boundary conditions in lower clamp and applied load in upper clamp are indicated.

SUR mesh, Equation 3.19.

Boundary conditions simulate the uniaxial test. Displacements are fixed in all directions in the lower clamp. In the upper side a preload of 2 N is applied and, after that, a displacement corresponding to a 100% of strain is imposed in the axial direction.

The response of the FE simulation considering the estimated material parameters and the experimental uniaxial tests are compared in order to validate the models.

Figures 4.3.a, 4.3.b and 4.3.c presents the curves from experimental uniaxial tests in both longitudinal and transversal directions and the results of the FE simulation for the three studied meshes. ECS vs. stretch are represented showing the good fit of the curves. Regarding to INF mesh FE simulation, the fitting of the longitudinal direction has a better agreement than the transversal and this fact is due to the high exponential character of the curves.

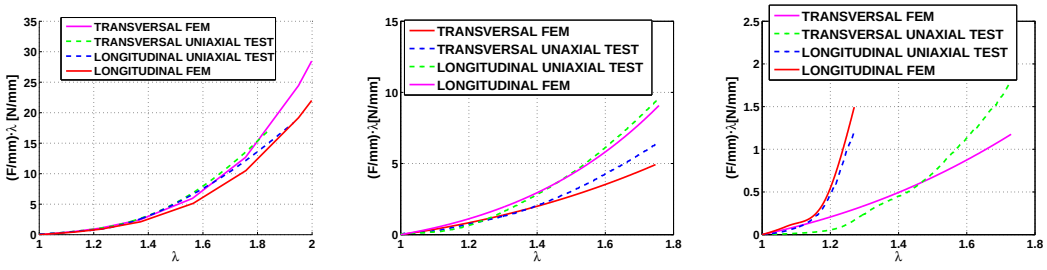

(a) (b) (c)

Figure 4.3: ECS vs. stretch for uniaxial test in longitudinal and transversal directions; experimental data and FE simulation. (a) SUR mesh. (b) OPT mesh. (c) INF mesh.

4.3 Simplified model of the abdominal cavity of the animal model

In order to reproduce the abdominal wall behaviour and to analyze the effect of the meshes in the abdominal wall, a simplified FEM simulation was developed considering the rabbit abdomen as a simplified geometry of an extruded ellipse. The dimensions of the geometry were determined based on measurements from the abdomen of rabbits weighting $2150 \pm 50g$. The long axis of the ellipse has a length of 140 mm and the short one 60 mm, Figure 4.4.a. The thickness of the complete abdomen was considered 3.5 mm and the length, coincident with the length of the rabbit abdomen, was fixed at 160 mm, Figure 4.4.a. The preferential direction of anisotropy for healthy muscle tissue was included in each element and this directions are drawn in Figure 4.5. Two lids in the upper and lower sides of the abdomen were included in order to reproduce the abdominal cavity, Figure 4.4.a and 4.4.b. Regarding to the boundary conditions, displacements from nodes placed in the back of the abdomen have been fixed in all directions to model the constrain of the shoulder, Figure 4.4.a. Finally, a pressure of 60 mmHg (8 kPa) [7] was imposed to the interior abdominal wall in order to reproduce abdominal load when standing Valsalva.

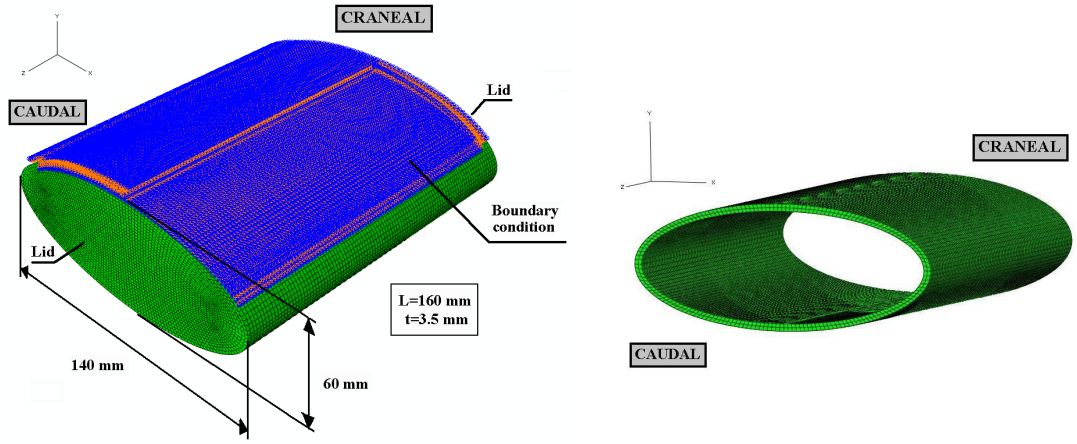

(a) (b)

Figure 4.4: (a) Simplified model of the rabbit abdomen where craneo-caudal direction and boundary conditions are indicated. (b) Simplified model when the lids are removed.

As a simplified model, the response of the abdominal muscle tissue was modelled using the material parameters indicated in Table 3.1 for EO-IO composite muscle layer. Considering the whole as healthy muscle, Figure 4.4, the total number of elements and nodes were 41856 and 62790, respectively. Linear hexahedral elements of type C3D8H

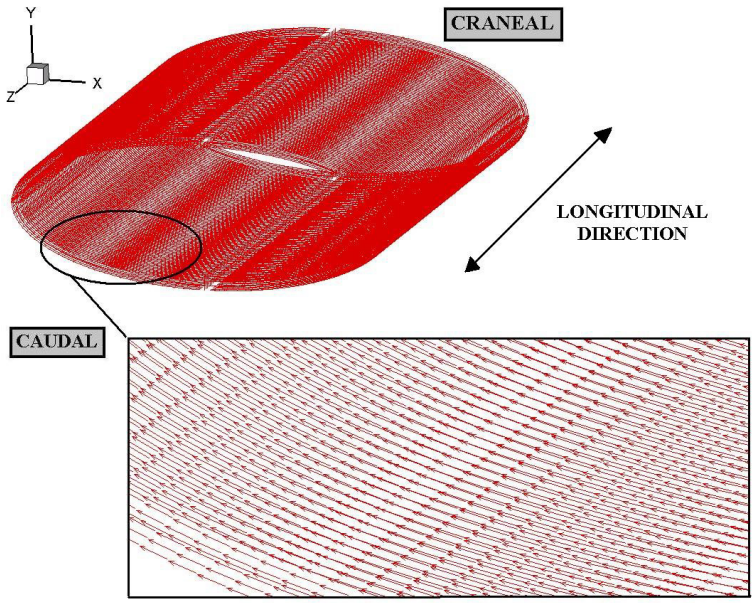

Figure 4.5: Preferential direction of anisotropy for healthy muscle tissue.

were chosen and the abdominal muscle tissue was implemented by a UMAT subroutine.

The most common hernia is the partial one which must be modelled as a lack of healthy tissue, which is replaced with a mesh, Figure 4.6.a. The hernia was provoked in the front of the abdomen, in the middle of the length of the abdomen and next to the linea alba, Figure 4.6.a. The dimensions were 40 x 40 mm. As a real example, Figure 4.6.b shows a SUR mesh that has been implanted and stitched in the rabbit abdomen. In this case, a total of 62376 nodes, 41400 linear hexahedral elements of type C3D8H for the abdominal wall and 456 linear hexahedral membrane elements of type M3D4 for the mesh were included. The M3D4 elements were coincident with the nodes below so the suture, placed in the limit of the mesh, is assumed to be continue. In this study SUR, OPT and INF implanted meshes were simulated. The material parameter used are included in Table 3.2 for SUR mesh and in Table 3.3 for OPT and INF meshes. SUR mesh was implemented through a material of the library of Abaqus and OPT mesh, INF mesh and abdominal muscle tissue were implemented by a UMAT subroutine.

In order to present results from simplified FEM simulation and to appreciate the internal area, one half of the model has been removed, Figures 4.7 and 4.8. In Figure 4.7 maximal principal stress are shown for the different studied cases and, in all cases, the highest values appear in the limit of the boundary condition in the back of the abdomen, Figure 4.4.a. However, based on the fact that the closest area to the hernia defect is the objective in this study, results are focussed on that zone. Besides, the same results are shown in Figure 4.9 but in a zoom view. Maximal principal stress in healthy abdominal

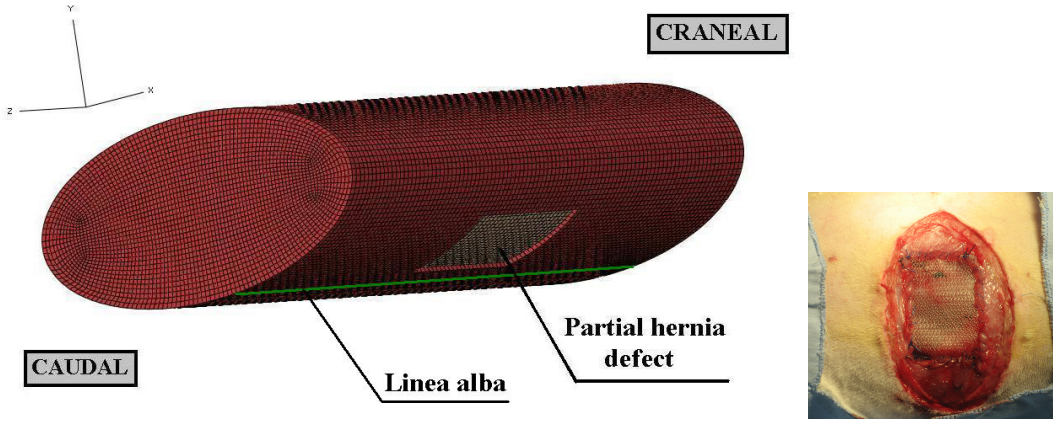

(a) (b)

Figure 4.6: (a) Simplified model of the rabbit abdomen with a partial hernia defect. (b) SUR mesh just implanted in the rabbit abdomen.

wall are referred in Figure 4.7.a and in the upper and left area of the Figure 4.9. Having an homogeneous distribution, the maximum principal stress in the front of the abdomen is about 0.196 MPa. In Figures 4.7.b, 4.7.c and 4.7.d the hernia defect is included and SUR, OPT and INF meshes are modelled respectively. Referring to SUR mesh and to the front of the abdomen, the maximum principal stress is 0.205 MPa and OPT mesh provoke a maximum value of the 0.2052 MPa. Finally, INF mesh reaches its maximum at 0.20224 MPa, Figure 4.7.d. The three surgical meshes have higher values of maximal principal stress in the front of the abdomen than in the healthy wall.

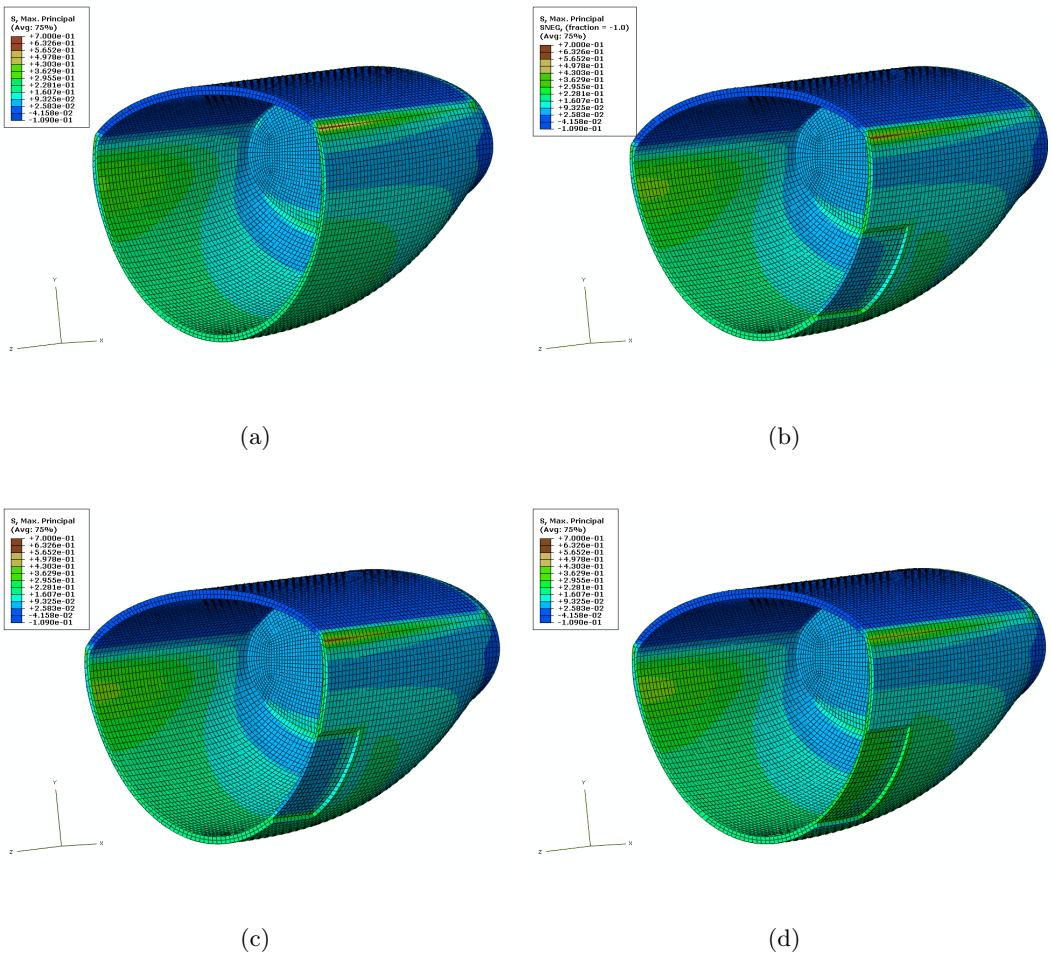

(a) (b)

(c) (d)

Figure 4.7: Maximal principal stress obtained in the simplified FEM simulation. (a) Healthy abdominal wall. (b)Healthy abdominal wall with SUR mesh. (c) Healthy abdominal wall with OPT mesh. (d) Healthy abdominal wall with INF mesh.

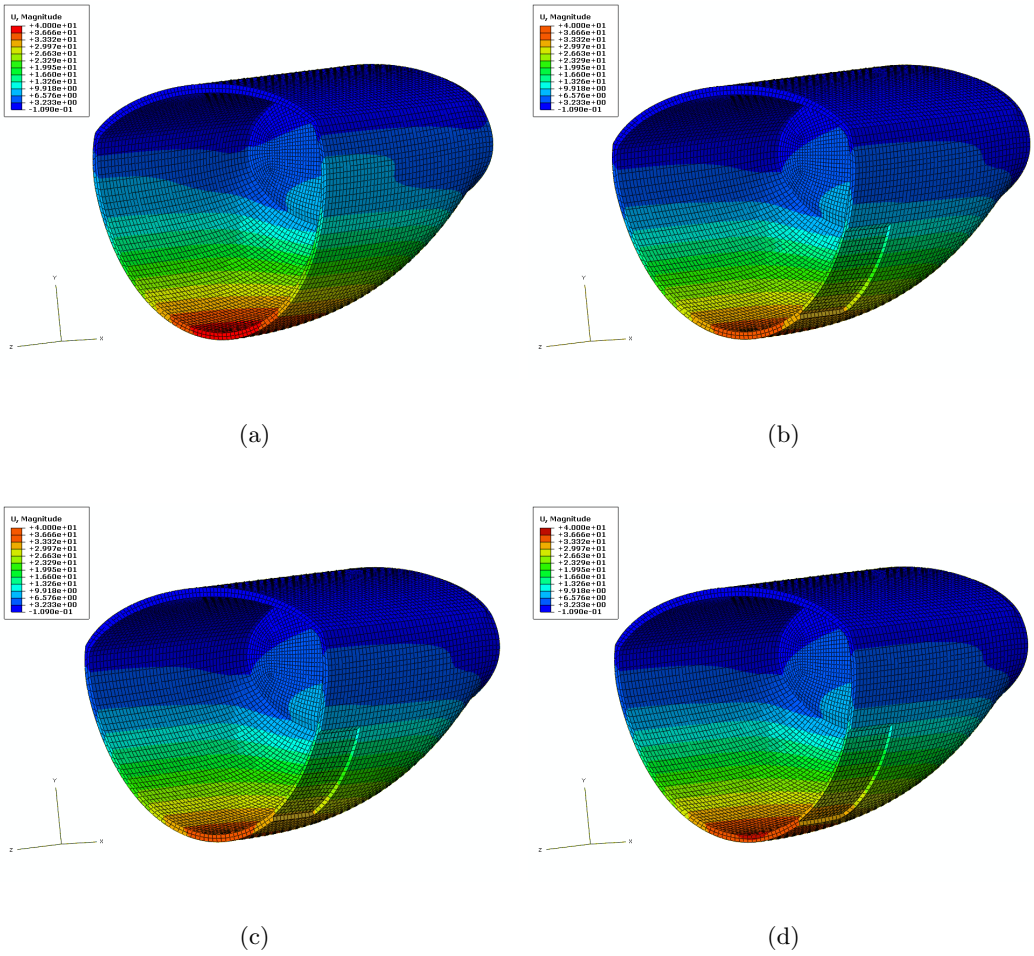

Figure 4.8: Maximal displacements obtained in the simplified FEM simulation. (a) Healthy abdominal wall. (b) Healthy abdominal wall with SUR mesh. (c) Healthy abdominal wall with OPT mesh. (d) Healthy abdominal wall with INF mesh.

Focussing on Figure 4.9 there is not an homogeneous distribution of maximal principal stress in the area of the hernia defect. In all three cases with an implanted mesh the stress rises up when approaching to the limit of the mesh or suture zone. Analyzing an element from the center of the mesh and in the INF simulation, it reaches 0.2413 MPa in the tissue and 0.2679 MPa in the mesh. When SUR is simulated, it reaches 0.08516 MPa in the tissue and 0.529571 MPa in the mesh. Finally, in OPT simulation, it provoke 0.07726 MPa in the tissue and 0.531979 MPa in the mesh. In the same reference element, healthy muscle tissue reaches 0.19277 MPa. In SUR y OPT cases the mesh supports more stress than the muscle tissue. In INF simulation maximal principal stresses are balanced between the muscle tissue and the mesh and this is probably due to the fact that INF mesh has a high anisotropic behaviour and it has been disposed in the opposite direction. Taking an element next to the limit of the mesh or suture zone, the maximum principal stress values that appear are 0.1562 MPa, 0.1492 MPa and 0.2804 MPa for SUR, OPT and INF meshes, respectively. Referring to healthy abdominal wall, the maximum value in this element is 0.2026 MPa, higher than SUR and OPT cases and lower than INF one.

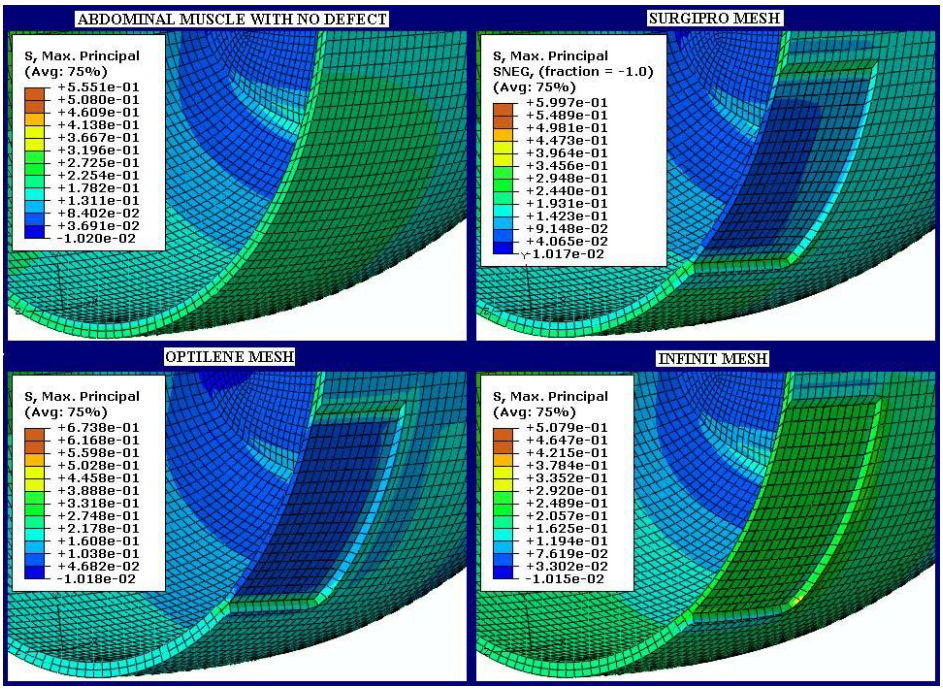

(a)

Figure 4.9: Maximal principal stress in the area of the hernia defect. Healthy abdominal wall with no defect and the three different and implanted meshes are compared.

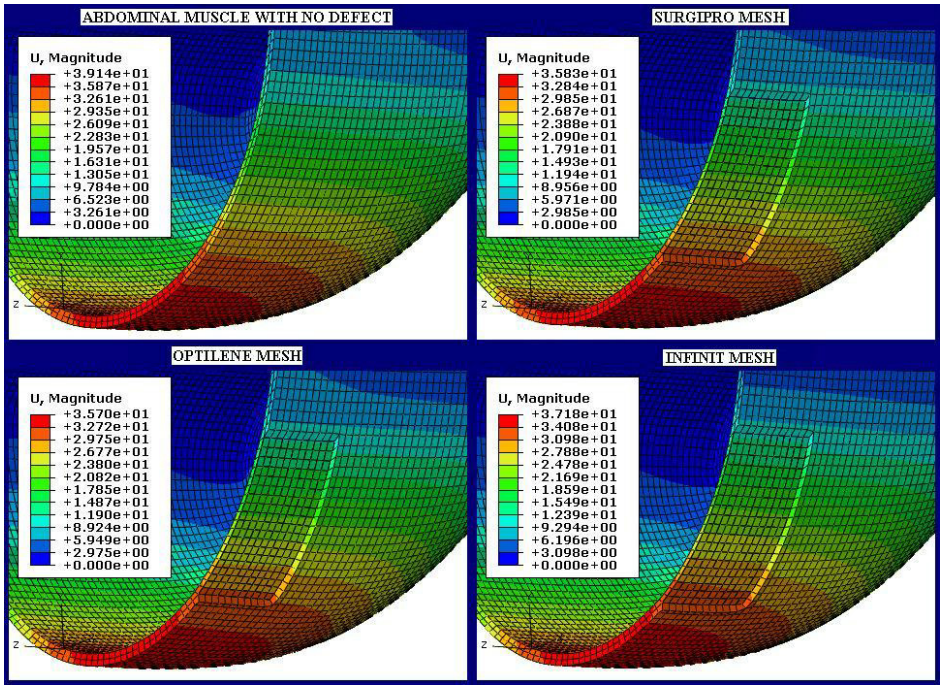

(a)

Figure 4.10: Maximal displacements in the area of the hernia defect. Healthy abdominal wall with no defect and the three different and implanted meshes are compared.

Furthermore, maximal displacements are very important so they are shown in Figure 4.8 and a zoom view is included in Figure 4.10. Regarding to Figure 4.8, red color only appears in Figure 4.8.a due to the fact that all meshes prevent original displacements making the abdomen stiffer. That is to say, no mesh is capable of reproduce real displacements of the healthy abdominal wall. Focussing on Figure 4.10 maximum values can be analyzed. In that case, the range of interest is shown in each legend, so the maximum value corresponds to the maximum displacement in the front of the abdomen. Healthy abdominal muscle reaches 39.14 mm, while SUR, OPT and INF surgical meshes provoke 35.83 mm, 35.70 mm, 37.18 mm, respectively.

To sum up, including a mesh into the healthy abdominal wall clearly provokes an alteration of the distribution of the maximal principal stresses. That means that surgical procedure does not solve the medical problem correctly since physiological conditions are not the same previous and after surgery. Not only the distribution is altered on the whole but also concentration of values appears in the area of the defect, being higher in the limit of the mesh or suture line, Figure 4.9. In the front of the abdomen, when a mesh has

been implanted, maximum ECS values are always higher than in healthy abdominal wall. The highest values take place with SUR and OPT meshes, while INF one is lightly lower. Focussing in the area of the hernia defect, only INF mesh provoke a stiffer response than healthy abdominal wall. On the other hand, maximum displacements are also altered by the implantation of the mesh. Once again, the maximum displacements take place in the healthy abdominal wall corroborating that surgical meshes contribute with a stiffer response. Comparing the three studied meshes, SUR and OPT behave in a similar way, letting similar displacements in the front of the abdomen while INF one reach higher values in that zone. As it has been mentioned, the disposition of the mesh in the abdomen is fundamental in order to get the perfect correspondence between abdominal wall and surgical mesh.

Chapter 5

Conclusions

5.1 Abdominal muscle tissue

In the present work, the passive elastic behaviour of the abdominal wall has been studied including initial strains. Several samples extracted from experimental animals were tested in order to characterize the mechanical properties of the abdominal wall, due to the importance for abdominal surgery for hernia repair and with the objective of reducing several problems caused by synthetic meshes [34, 3]. The mechanical properties and initial strains were then evaluated using the classical rabbit model for these kinds of pathologies.

Biological soft tissues are usually exposed to a complex distribution of *in vivo* initial strains due to the continuous growth, remodelling, damage and viscoplastic strains that suffer these living materials throughout their whole lives. In this study, shortening of the tissue along different directions was measured to estimate these initial strains. After contraction the shape of the specimen remained approximately rectangular which indicates that the specimen has been taken more or less along its principal material axes.

As can be seen in the literature [9], for good clinical results in abdominal hernia surgery, a perfect correspondence is required between the mechanical properties of the abdominal wall and the mechanical properties of the biomaterial used for repair. Other studies can be found in the literature related to abdominal wall behaviour, each of them focussing on similar aspects but not directly comparable with the present results. On the one hand,a comparative study has been carried out between IO and TA canine muscles [19], while here both are studied as a composite. In cited paper, similar conclusions are obtained in terms of anisotropy and muscle compliance comparing a single muscle layer and a composite. On the other hand, mechanical properties of specimens from different anatomical positions as well as in relation to geometric variables and fibre orientation have also been studied, [30, 31]. Nilsson [30, 31] obtained results relating force and stretch but no data referring

to cross sectional area were given, so stress data could not be obtained and therefore the results cannot be compared with the presented in this study. Nevertheless, the stress-stretch relationships obtained in the present study showed similar non-linear patterns to those previously published for soft tissues in general, also undergoing large deformations [19, 25, 38, 10, 28, 6].

As regards to passive behaviour, both, the EO muscle layer and the IO-TA bilayer demonstrated a stiffer behaviour along the transversal direction to muscle fibres than along the longitudinal one. The fibre arrangement obtained in histologies confirm that collagen fibres are principally responsible for passive mechanical strength and stiffness. Considering the muscle as a whole composite, the transversal direction is the stiffer one. Also, the degree of anisotropy of the abdominal composite muscle turned out to be less pronounced than those obtained while studying the EO and IO-TA separately.

As discussed previously, the abdominal muscles are arranged in multiple layers, each with collagen and muscle fibres oriented along a different axis from that of the adjacent layer. In the presence of extracellular connective tissue matrix, this arrangement of muscle layers allows for the transmission of muscle forces between adjacent muscle layers called myofascial force transmission [19]. Therefore, rather than bearing a transverse stress with increased abdominal pressure during inspiratory activity, muscle layers can transmit this transverse stress to the adjacent abdominal muscle layer. Due to this fact, composites behave in an intermediate way between single muscle layers, Figure 2.9.b and 2.9.c.

Referring to the model formulation, a constitutive model has been proposed that can be used to study muscle tissue mechanics. Figure 3.2 indicates that this constitutive model is sufficiently accurate to guarantees the prediction of reliable stress distributions using finite element computations. The good fit in the range of the physiological work guarantee the correct response of the tissue in FE simulations. To demonstrate this, a FE simulation with Abaqus has been developed, Figure 4.1.a. The correspondence between the two FE models and experimental results validates the assumption, so it is possible to simulate the tissue as a composite or as two separate muscle layers using the material parameters previously fitted, Table 3.1.

5.2 Surgical meshes

In the present work, the mechanical behaviour of three kind of meshes have been analyzed through experimental uniaxial tests. A material model by a SEF for each mesh was proposed and the material parameters was fitted. After that, a FE simulation of the experimental test was computed to validate the material model chosen. Finally, these properties have been included in a simplified model of the rabbit abdomen.

To the authors' knowledge, there is no similar study that includes all the steps described here for the surgical meshes. Some authors have studied the response of some meshes but

always focusing in the evolution of the mesh before and after a period of time from the implant [4, 34, 8]. Afonso et al. [1] studied five different meshes under two types of mechanical test, uniaxial and compression tests, but the meshes were not the same as those studied here.

The experimental data of surgical meshes presented in this work show that SUR mesh presents an isotropic mechanic response while OPT and INF meshes present an anisotropic behaviour. Both, OPT and INF meshes are stiffer in longitudinal direction, Figure 2.10, and this fact has been justified previously based on the spatial arrangement of the filaments. Consequently, in order to get a perfect mechanical correspondence between abdominal wall and the surgical meshes used for hernia repair, the stiffer direction of the surgical mesh, Figure 2.10, must be disposed in the transversal direction of the abdomen, Figure 2.1. So both, OPT and INF meshes should be disposed in the opposite direction in order to have similar mechanical response. Referring to SUR mesh, the orientation does not matter based on its isotropic response. However, the longitudinal direction of the muscle tissue has not a good agreement when choosing SUR nor OPT mesh because they are stiffer.

Referring to the model formulation, a 2D constitutive model has been proposed that can be used to study surgical meshes mechanics. Figure 4.3 indicates that this membrane model is sufficiently accurate to guarantees the prediction of reliable stress distributions using finite element computations.

The simplified FE simulations include the muscle tissue and the biomaterial used for hernia repair. As a first approximation to the modelling of the hernia defects, only partial hernias, which takes place when there is a lack of tissue in the EO muscle layer, are considered. Actually, partial hernia defects are the most common defects in human body. Based on the fact that muscle tissue can be simulated as a composite or as two separate muscle layers, the healthy muscle tissue is considered as a continuous composite muscle. As discussed previously, including a mesh into the healthy abdominal wall when a partial hernia defect takes place clearly provokes an alteration of the original mechanical response due to the fact that stresses increase and the displacement of the abdomen decreases. That means that surgical procedure does not solve the medical problem correctly since physiological conditions are not the same previous and after surgery. Furthermore, the highest concentration of stress takes place in the continue suture of the mesh.

Chapter 6

Future work

Referring to the abdominal muscle tissue characterization, some limitations should be mentioned. Only the elastic properties of the tissues have been determined here. Damage and viscoelastic properties were not included and remain issues for subsequent work [6, 35]. Further tests are needed to determine the plastic and viscoelastic properties of muscle, as well as the stiffness loss due to damage. Further information from other kinds of tests (e.g. biaxial tests) would provide useful additional information for muscle tissue characterization. Moreover, biaxial tests reproduce the physiological deformation and loading conditions of muscle tissue. Besides, subsequent work will include the characterization of active behavior which may provide additional information for muscle tissue. Despite these limitations, the proposed constitutive model can be used to study muscle tissue mechanics as it seems to be sufficiently accurate to guarantee the prediction of reliable stress distributions using finite element computations.

On the other hand, referring to surgical meshes characterization, some limitations should also be mentioned. In the study, ECS vs. stretch is always represented due to the fact that the objective was to eliminate the dependence of the thickness. Working with Cauchy stress vs. stretch in the muscle tissue characterization is the same if a thickness of $1mm$ is considered. The fact of establishing the thickness of the meshes is very difficult because there is not a continuous surface. Besides, further information from other kind of test (e.g. biaxial test) would provide useful additional information for the characterization of the meshes, as well as in muscle tissue characterization, due to the fact that biaxial tests reproduce the physiological deformation and loading conditions of the surgical meshes. Besides, the study of the remodeling of the tissue and the growth of the collagen after implanting the mesh is convenient since that issue probably will cause important changes into stiffness. Another limitation of this study is the simplified geometry of the rabbit abdomen and that could be improved taking scan images from experimental

animals or humans. Despite these limitations, the study is a solid step which establish the mechanical properties of three different and commercial surgical meshes. After the mechanical comparison between healthy abdominal muscle and surgical meshes should be possible to establish some guidelines to the surgeons, so that the correct disposition of the mesh was chosen.

Further studies will include the FE simulation of surgical meshes through beam models (B31 elements) in order to reproduce the geometry of the mesh perfectly. That way, the weave of the mesh could be taken into account. Future designs of surgical meshes could be simulated in order to analyze the mechanical response. Figure 6.1 shows the geometry of SUR and OPT meshes by means of beam elements in Abaqus code. Figures 6.1.a and 6.1.c show the unit cells and Figures 6.1.b and 6.1.d show four cells for each mesh.

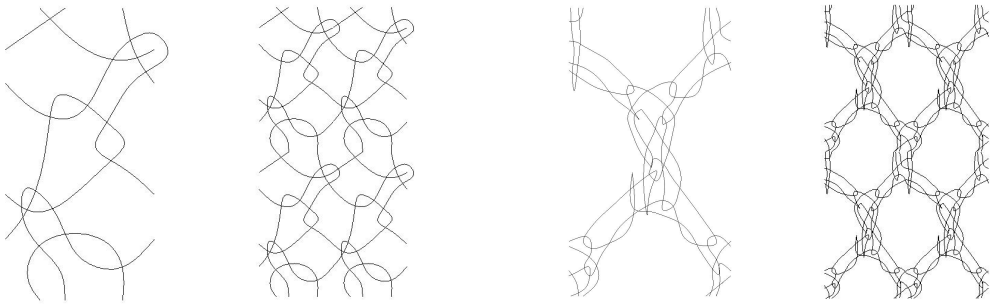

(a) (b) (c) (d)

Figure 6.1: FE model of SUR and OPT meshes with B31 elements. (a) One SUR unit cell (1.1 mm x 2.155 mm) . (b) Four SUR unit cells. (c) One OPT unit cell (2.86 mm x 5.11 mm) . (b) Four OPT unit cells.

Besides, further studies would include the evolution of the behaviour of the abdominal wall once mesh was implanted and after different periods of time. In that case, mechanical properties as well as histologies should be studied and correlated in order to understand the remodelling of the tissue and the growth of the collagen that probably will depend on the pore size and spatial distribution of the surgical meshes.

Chapter 7

Acknowledgments

I gratefully acknowledge research support from the Spanish Ministry of Science and Technology through the research project DPI2008-02335 and the Instituto de Salud Carlos III (ISCIII) through the CIBER initiative project SOFT-TISSUES-BIOSCAFF. CIBER-BBN is an initiative funded by the VI National R&D&i Plan 2008-2011, Iniciativa Ingenio 2010, Consolider Program, CIBER Actions and financed by the Instituto de Salud Carlos III with assistance from the European Regional Development Fund.

Besides, I also thank the Spanish Ministry of Science and Technology for the financial support to B. Hernández through the grant BES-2009-021515.

Finally, I acknowledge the departments of Surgery and Medical Specialities, Faculty of Medicine, of University of Alcalá, for the grant I received in order to do a research stay working with J. M. Bellón, G. Pascual and M. Rodríguez. I have understood the clinical problem working with them.

Bibliography

[1] Afonso, J., Martins, P., Girao, M., Natal Jorge, R., Ferreira, A., Mascarenhas, T., Fernandes, A., Bernardes, J., Baracat, E., Rodrigues de Lima, G., Patricio, B., 2008. Mechanical properties of polypropylene mesh used in pelvic floor repair. International Urogynecology Journal 19, 375–380.

[2] Arruda, E. M., Mundy, K., Calve, S., Baar, K., 2006. Denervation does not change the ratio of collagen I and collagen II mRNA in extracellular matrix of muscle. American Journal of Physiology - Regulatory, Integrative and Comparative Physiology 292, 983–987.

[3] Bellón, J. M., 2009. Role of the new lightweight prostheses in imporving hernia repair. Cirugía española 85(5), 268–273.

[4] Bellón, J. M., Rodríguez, M., García-Honduvilla, N., Gómez-Gil, V., Pascual, G., Buján, J., 2009. Comparing the behavior of different polypropylene meshes (heavy and lightweight) in an experimental model of ventral hernia repair. Journal of Biomedical Materials Research. Part B, Applied Biomaterials 89B(2), 448–55.

[5] Bol, M., Reese, S., 2008. Micromechanical modelling of skeletal muscles based on the finite element method. Computer Methods in Biomechanics and Biomedical Engineering 11, 489 – 504.

[6] Calvo, B., Peña, E., Martins, P., Mascarenhas, T., Doblare, M., Natal, R., Ferreira, A., 2009. On modelling damage process in vaginal tissue. Journal of Biomechanics 42, 642–651.

[7] Cobb, W. S., Burns, J. M., Kercher, K. W., Matthews, B. D., Norton, H. J., Heniford, B. T., 2005. Normal Intraabdominal Pressure in Healthy Adults. Journal of Surgical Research 129, 231–235.

[8] Cobb, W. S., Burns, J. M., Peindl, R. D., Carbonell, A. M., Matthews, B. D., Kercher, K. W., Heniford, B. T., 2006. Textile analysis of heavy-weight, mid-weight and light-weight polypropylene mesh in a porcine ventral hernia model. Journal of Surgical Research 136, 1–7.

[9] Conze, J., Klinge, U., 1999. Biocompatibility of biomaterials-clinical and mechanical aspects. Springer, Berlin, Heidelberg, New York, Ch. 14, pp. 169–177.

[10] Davis, J., Kaufman, K. R., Lieber, R. L., 2003. Correlation between active and passive isometric force and intramuscular pressure in the isolated rabbit tibialis anterior muscle. Journal of Biomechanics 36 (4), 505–512.

[11] Demiray, H., Weizsacker, H. W., Pascale, K., Erbay, H., 1988. A stress-strain relation for a rat abdominal aorta. Journal of Biomechanics 21, 369–374.

[12] DeTroyer, A., Lohring, S. H., 1986. Handbook of Physiology. The Respiratory System. Mechanics of Breathing. Vol. 3. The American Physiological Society, Ch. Action of the respiratory muscles, pp. 443–461.

[13] E. K, J., Hoyt, C. H., Dinsmore, R. C., 2004. Abdominal wall hernia repair: a long-term comparison of sepramesh and dualmesh in a rabbit hernia model. American Journal of Surgery 70(8), 657–61.

[14] Fernandez, J. W., Pandy, M. G., 2006. Integrating modelling and experiments to assess dynamic musculoskeletal function in humans. Experimental Physiology 91 (2), 371–382.

[15] Gardiner, J. C., Weiss, J. A., 2003. Subjet-specific finite element analysis of the human medial collateral ligament during valgus knee loading. Journal of Orthopaedics Research 21, 1098–1106.

[16] Holzapfel, G. A., 2000. Nonlinear Solid Mechanics. Wiley, New York.

[17] Holzapfel, G. A., Gasser, C. T., Sommer, G., Regitnig, P., 2005. Determination of the layer-specific mechanical properties of human coronary arteries with non-atherosclerotic intimal thickening, and related constitutive modelling. American Journal of Physiology-Heart and Circulatory Physiology 289, H2048–H2058.

[18] Holzapfel, G. A., Gasser, T. C., Ogden, R. W., 2000. A new constitutive framework for arterial wall mechanics and a comparative study of material models. Journal of Elasticity 61, 1–48.

[19] Hwang, W., Carvalho, J. C., Tarlovsky, I., Boriek, A. M., 2005. Passive mechanics of canine internal abdominal muscles. Journal of Applied Physiology 98 (5), 1829–1835.

[20] Jenkyn, T. R., Koopman, B., Huijing, P., Lieber, R., Kaufman, K. R., 2002. Finite element model of intramuscular pressure during isometric contraction of skeletan muscle. Physics in Medicine and Biology 47(22), 4043–61.

[21] Judge, T. W., Parker, D. M., Dinsmore, R. C., 2007. Abdominal wall hernia repair: a comparison of sepramesh and parietex composite mesh in a rabbit hernia model. Journal of the American College of Surgeons 204(2), 276–81.

[22] Klinkel, S., Govindjee, S., 2002. Using finite strain 3D-material models in beam and shell elements. Engineering Computations 19(8), 902–921.

[23] LeBlanc, K. A., Bellanger, D., 5th, K. V. R., Baker, D. G., Stout, R. W., 2002. Tissue attachment strength of prosthetic meshes used in ventral and incisional hernia repair. A study in the New Zealand White rabbit adhesion model. Surgical Endoscopy 16(11), 1542–6.

[24] Linden, V. D., 1998. Mechanical modeling of skeletal muscle functioning. Ph.D. thesis, University of Twente, The Netherlands.

[25] Lopez, M., Pardo, P., Cox, G., Boriek, A., 2008. Early mechanical dysfunction of the respiratory pump in the muscular dystrophy with myositis (ttn^{mdm}) model. American Journal of Physiology-Cell Physiology 295, C1092 – C1102.

[26] Marquardt, D. W., 1963. An algorithm for least-squares estimation of nonlinear parameters. SIAM Journal on Applied Mathematics 11, 431–441.

[27] Martins, J., Pires, E., Salvado, R., Dinis, P., 1998. A numerical model of passive and active behavior of skeletal muscles. Computer Methods in Applied Mechanics and Engineering 151, 419–433.

[28] Martins, P., Peña, E., Calvo, B., Doblaré, M., Mascarenhas, T., Jorge, R. N., Ferreira, A., 2010. Prediction of nonlinear elastic behavior of vaginal tissue: Experimental results and model formulation. Computer Methods in Biomechanics and Biomedical Engineering , 327–337.

[29] Miller, M. E., 1993. Miller's Anatomy of the Dog. Saunders, Philadelphia.

[30] Nilsson, T., 1982. Biomechanical studies of rabbit abdominal wall. Part I.- The mechanical properties of specimens from different anatomical positions. Journal of Biomechanics 15 (2), 123–129.

[31] Nilsson, T., 1982. Biomechanical studies of rabbit abdominal wall. Part II.- The mechanical properties of specimens in relation to length, width, and fibre orientation. Journal of Biomechanics 15 (2), 131–135.

[32] Odegard, G. M., Donahue, T. L. H., Morrow, D. A., Kaufman, K. R., 2008. Constitutive modeling of skeletal muscle tissue with an explicit strain-energy function. ASME Journal of Biomechanical Engineering 130, 061017.

[33] Ogden, R. W., 2001. Nonlinear Elasticity, Anisotropy, Material Stability and Residual Stresses in Soft Tissue. Lecture Notes, CISM. Course on Biomechanics of Soft Tissue, Udine.

[34] Pascual, G., Rodríguez, M., Gómez-Gil, V., García-Honduvilla, N., Buján, J., Bellón, J. M., 2008. Early tissue incorporation and collagen deposition in lightweight polypropylene meshes: bioassay in an experimental model of ventral hernia. Surgery 144(3), 427–35.

[35] Peña, E., Calvo, B., Martínez, M. A., Martins, P., Mascarenhas, T., Jorge, R. M. N., Ferreira, A., Doblare, M., 2010. Experimental study and constitutive modeling of the viscoelastic mechanical properties of the human prolapsed vaginal tissue. Biomechanics and Modeling in Mechanobiology 9, 35–44.

[36] Peña, E., Calvo, M. A. M. B., Doblaré, M., 2006. On the numerical treatment of initial strains in soft biological tissues. Int J Numer Meth Engng 68, 836–860.

[37] Peña, E., del Palomar, A. P., Calvo, B., Martínez, M. A., Doblaré, M., 2007. Computational modelling of diarthrodial joints. Physiological, pathological and pos-surgery simulations. Archives of Computational Methods in Engineering 14(1), 47–91.

[38] Quapp, K. M., Weiss, J. A., 1998. Material characterization of human medial collateral ligament. ASME Journal of Biomechanical Engineering 120, 757–763.

[39] Rosch, R., Junge, K., Hölzl, F., Schachtrupp, A., Stumpf, M., Klinge, U., 2004. Meshes: Benefits and risks. Springer-Verlag, Ch. How to construct a mesh? Impact of structure, filament and pore size for tissue ingrowth, pp. 179–188.

[40] Schippers, E., 2007. Recurrent hernia. Springer Berlin Heidelberg, Ch. Central mesh rupture- Myth or real concern?, pp. 371–376.

[41] Simo, J. C., Taylor, R. L., 1991. Quasi-incompresible finite elasticity in principal stretches. Continuum basis and numerical algorithms. Computer Methods in Applied Mechanics and Engineering 85, 273–310.

[42] Spencer, A. J. M., 1954. Theory of invariants. In: Continuum Physics. Academic Press, New York, pp. 239–253.

[43] Stalhand, J., Klarbring, A., Holzapfel, G. A., 2008. Smooth muscle contraction: mechanochemical formulation for homogeneous finite strains. Progress in Biophysics & Molecular Biology 96, 465–481.

[44] Weiss, J. A., Maker, B. N., S.Govindjee, 1996. Finite element implementation of incompressible, transversely isotropic hyperelasticity. Computer Methods in Applied Mechanics of Engineering 135, 107–128.